Micropolar Elasticity in Physically-Based Animation

FABIAN LÖSCHNER, RWTH Aachen University, Germany
JOSÉ ANTONIO FERNÁNDEZ-FERNÁNDEZ, RWTH Aachen University, Germany
STEFAN RHYS JESKE, RWTH Aachen University, Germany
ANDREAS LONGVA, RWTH Aachen University, Germany
JAN BENDER, RWTH Aachen University, Germany

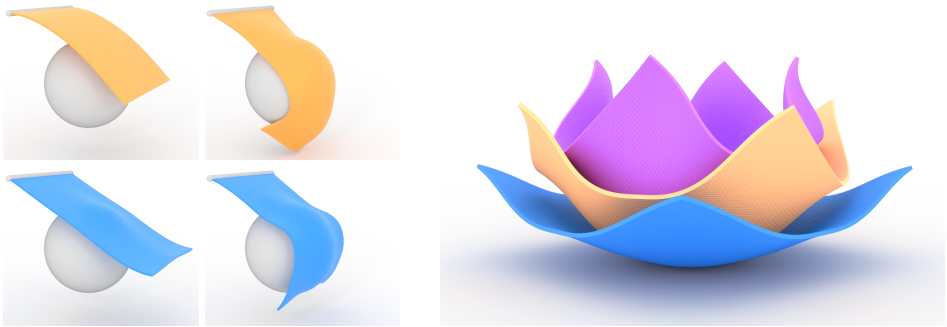

Fig. 1. Two example applications of micropolar materials in computer graphics. Left: A thin clamped sheet collides with a sphere and bends. With classic isotropic elasticity (top row) the sheet can either be stiff, and therefore nearly inextensible ($E = 1 \cdot 10^7$ Pa), or soft and stretchy ($E = 2 \cdot 10^4$ Pa). However, micropolar materials can simultaneously be extensible ($E = 2 \cdot 10^4$ Pa) and stiff to bending ($\mu_c = \mu$, $L_c = 1$). Further, bending stiffness can be isotropic (bottom left, $\alpha = \beta = \gamma = 20$) or anisotropic (bottom right, $\mathbf{C}_{xy} = 20$). Right: The rest pose curvature of three thin sheets, starting from a flat initial pose, is modified to induce internal stresses that result in large deformations and end up forming a lotus-like shape.

We explore micropolar materials for the simulation of volumetric deformable solids. In graphics, micropolar models have only been used in the form of one-dimensional Cosserat rods, where a rotating frame is attached to each material point on the one-dimensional centerline. By carrying this idea over to volumetric solids, every material point is associated with a *microrotation*, an independent degree of freedom that can be coupled to the displacement through a material's strain energy density. The additional degrees of freedom give us more control over bending and torsion modes of a material. We propose a new orthotropic micropolar curvature energy that allows us to make materials stiff to bending in specific directions.

For the simulation of dynamic micropolar deformables we propose a novel incremental potential formulation with a consistent FEM discretization that is well suited for the use in physically-based animation. This allows us to easily couple micropolar deformables with dynamic collisions through a contact model inspired from the Incremental Potential Contact (IPC) approach. For the spatial discretization with FEM we discuss the challenges related to the rotational degrees of freedom and propose a scheme based on the interpolation of angular velocities followed by quaternion time integration at the quadrature points.

In our evaluation we validate the consistency and accuracy of our discretization approach and demonstrate several compelling use cases for micropolar materials. This includes explicit control over bending and torsion stiffness, deformation through prescription of a volumetric curvature field and robust interaction of micropolar deformables with dynamic collisions.

SCA '23, August 04–06, 2023, Los Angeles, CA

CCS Concepts: • **Computing methodologies** → **Physical simulation**.

Additional Key Words and Phrases: micropolar materials, cosserat continuum, elasticity, physically-based simulation, optimization time integration

ACM Reference Format:
Fabian Löschner, José Antonio Fernández-Fernández, Stefan Rhys Jeske, Andreas Longva, and Jan Bender. 2023. Micropolar Elasticity in Physically-Based Animation. In *Proceedings of the ACM on Computer Graphics and Interactive Techniques, Volume 6, Issue 3.* ACM, New York, NY, USA, Article 1, 25 pages. https://doi.org/10.1145/3606922

1 INTRODUCTION

Classical hyperelastic displacement-based constitutive laws, such as the St. Venant-Kirchhoff and Neo-Hookean models, define strain energy densities $\Psi(\mathbf{F})$ that depend only on the deformation gradient $\mathbf{F}$ at each material point. This is sufficient for modeling a wide range of natural and interesting deformation, including realistic response to twisting and bending. Fundamentally, however, resistance to bending and torsion only happens in the aggregate; individual material points have no concept of torsion or bending. Therefore, an object's ability to resist bending and torsion is a consequence of the elastic stiffness and geometry of the object.

A lesser known class of materials are *micropolar materials*. In contrast to classical models, micropolar materials have additional *microstructure* in the form of a rotating frame attached to every material point. This rotating frame can be represented by a *microrotation* $\overline{\mathbf{R}}$ relative to the reference frame, and is typically coupled with displacements through the strain energy density $\Psi(\mathbf{F}, \overline{\mathbf{R}})$. The added microrotation gives each material point a measure of "volumetric curvature", which makes it possible to define strain energies that resist bending and torsion at each material point of the volume.

Inspired by these intriguing properties of micropolar materials, we present an exploratory study of micropolar models for use in graphics. We go beyond the physics and study artificial materials with rotational microstructure, which we show can produce a number of interesting effects when employed in dynamical simulation of deformables.

For example, whereas classical displacement-based materials must fundamentally choose between stiffness and softness, we show in Section 5.2 that micropolar materials can take on soft characteristics while simultaneously being resistant to bending. In Figure 4 and the supplemental video, we demonstrate how a volumetric hollow bunny remains soft to stretching, yet it is resistant to bending, and therefore does not collapse under its own weight like the classical Neo-Hookean material. We also demonstrate how the microstructure can be used to gradually induce curvature in the material, like the helices in Figure 6 and the lotus flower in Figure 1.

In order to study micropolar materials for dynamic deformables, we develop a novel finite element discretization in which we spatially interpolate angular velocities on the nodes to circumvent difficulties of directly interpolating rotations (Section 4.2). We integrate the discretization in an Incremental Potential formulation of Backward Euler (Section 4.1), which enables us to model dynamic collisions of micropolar solids with an IPC-inspired contact model [Li et al. 2020]. We also develop a novel intuitive orthotropic curvature energy that can be used as an alternative to the isotropic micropolar curvature energy commonly found in the mechanics literature (Section 3.3.2). The orthotropic curvature energy allows us to make deformables stiffer to bending in specific directions, which can be used to phenomenologically model more complex materials, for example with directional fibers or hole patterns. In Section 5, we demonstrate experimentally the consistency of our discretization, and contrast the behavior of our micropolar material models to classical models in a number of experiments.

2 RELATED WORK

Dynamic deformables in graphics. In physically-based animation, several approaches for the simulation of elastic deformables in multi-physics systems are established today. This includes Position-based dynamics [Bender et al. 2014; Müller et al. 2006], XPBD [Macklin and Müller 2021; Macklin et al. 2016] and Projective Dynamics [Bouaziz et al. 2014; Narain et al. 2016; Overby et al. 2017]. In recent years, incremental potential formulations (also known as optimization time integration [Gast et al. 2015; Kane et al. 2000; Kharevych et al. 2006]) combined with the Finite Element Method (FEM) for the spatial discretization of elastic bodies [Kim and Eberle 2022; Sifakis and Barbic 2012] gained popularity. Especially for challenging contact problems, the Incremental Potential Contact (IPC) approach [Li et al. 2020] built on these concepts proved to be very successful. Subsequently IPC was extended, e.g, to support coupling with co-dimensional deformables, rigid bodies and joints [Chen et al. 2022; Ferguson et al. 2021; Li et al. 2021]. In this work we will present an incremental potential formulation of micropolar elasticity with a consistent FEM discretization. This allows us to solve the dynamic problem using robust optimization methods and to couple our micropolar model with an IPC-inspired contact model.

Rotation DOFs in graphics. A core component of micropolar elasticity is the introduction of explicit rotational degrees of freedom in addition to the displacements known from classic elasticity. In the graphics community, the explicit use of rotational degrees of freedom was proposed by Müller and Chentanez [2011] to make shape matching more robust for the simulation of rigid, soft and plastic bodies in the context of PBD. However, this approach is quite specific for PBD and the rotations are not used for material modeling purposes. Recently, Brown and Narain [2021] proposed an ADMM solver and Trusty et al. [2022] a mixed FEM formulation for nonlinear elastic deformables which are explicitly rotation aware to improve robustness and convergence for large deformations under wide ranges of material and simulation parameters. Again, the rotation information does not introduce any new material modelling capabilities and the methods are therefore orthogonal to our work on micropolar material models.

Bending in deformable solids. Explicitly considering bending or curvature to model the behavior of deformables is mostly limited to shells and rods in physically-based animation (see e.g. [Bergou et al. 2006; Grinspun et al. 2003]). A notable special case is the concept of "elastons" proposed by Martin et al. [2010] which acts as a sort of integration rule with a single strain energy density for a unified formulation of rods, shells and volumetric deformables. However, while the elaston approach generally incorporates bending terms they are explicitly designed to vanish in the limit of refinement for volumetric solids. Micropolar materials instead introduce a notion of bending also for volumetric bodies in the continuum setting using explicit rotational degrees of freedom that are not present in the elaston model. In this sense, the concept of elastons is orthogonal to micropolar material models and one could potentially extend elastons to unify the implementation for micropolar solids, shells and rods as well.

Micropolar theory in graphics. In computer graphics, the theory of micropolar materials is nearly exclusively established in the form of Cosserat rods. These were initially introduced to the graphics community by Pai [2002] and inspired many works in subsequent years such as improvements for the robust dynamic simulation with self-contact [Spillmann and Teschner 2007], nets of rods linked with elastic joints [Spillmann and Teschner 2009], efficient simulation using PBD [Kugelstadt and Schömer 2016; Umetani et al. 2014], stiff and inextensible rods in XPBD [Deul et al. 2018] as well as volume invariant generalized rods, e.g., for the simulation of muscles and muscle groups [Angles et al. 2019]. To our knowledge the only work inspired by micropolar theory in a different domain of physically-based animation is the micropolar turbulence model for SPH fluids proposed by Bender

et al. [2017] which uses extra rotational degrees of freedom in a fluid to dynamically introduce more turbulent details.

Foundations of micropolar media. In mechanics, the foundations for micropolar materials were originally introduced by the Cosserat brothers [Cosserat and Cosserat 1909] who explored the kinematic relations of rods, shells and three-dimensional bodies involving additional rotational degrees of freedom. The classic models of Reissner-Mindlin plates [Neff et al. 2010], Timoshenko beams and Kirchhoff rods [O'Reilly 2017] can all be derived from this theory. Constitutive relations for such materials were introduced much later and an overview is provided, e.g., by Eringen [1999] and Eremeyev et al. [2012]. The properties of the variational problems associated with micropolar elasticity are not as well-studied as for classic elasticity but existence proofs of solutions can be found in the literature [Neff et al. 2015; Tambača and Velčić 2010]. In practice, micropolar material models are used to simulate deformable materials under the influence of external magnetic fields [Dadgar-Rad and Hossain 2023; Münch et al. 2011], granular materials [Walsh and Tordesillas 2006], porous media [Diebels 1999], phenomena from geomechanics [Abreu and Durand 2021; Manzari 2004], crystals [Abreu et al. 2018; Neff 2006], blood flow [Mekheimer and Kot 2008] and more.

Micropolar FEM. While fully nonlinear micropolar models were introduced in the past [Bauer et al. 2012; Ramezani et al. 2009], the use of so-called "physically linear" micropolar models is much more widespread. The forces of the latter models are linear in the deformation gradient but the overall problem is still nonlinear due to the coupling with rotations [Neff 2006]. In contrast to classic linear elasticity, the physically linear micropolar models can still be applied for large deformations. In mechanics the spatial discretization is commonly performed using FEM. The displacement field is usually discretized the same way as for classic elasticity, however it was suggested to enhance linear elements with "incompatible modes" (e.g. quadratic contributions) for the deformation field to improve convergence in scenarios dominated by strong bending [Grbčić et al. 2018]. The nodal microrotations are commonly interpolated using direct linear interpolation of rotation vectors [Bauer et al. 2010; Münch 2007]. As this often requires the conversion between rotation representations, Ghiba et al. [2022] recently proposed a formulation entirely in terms of skew-symmetric matrices related to rotation vectors which does not require explicit conversions. While the continuous micropolar model supports arbitrary rotations, the linear interpolation of rotation vectors introduces errors due to the nonlinear structure of the group of rotations $SO(3)$. An alternative approach is Geodesic FEM [Sander 2012, 2015] which is a general purpose discretization approach that accurately interpolates degrees of freedoms with manifold structure. The overall numerical framework required to apply Geodesic FEM, however, is very involved and computationally expensive. In computer animation, especially for skinning, Quaternion Linear Blending (QLB or QLERP) [Kavan and Žára 2005] is an established method to blend between multiple rotations. Due to drawbacks discussed in more detail in Section 4.2.1, we instead propose a discretization based on incremental rotations, or more specifically the interpolation of angular velocities which fits well into our incremental potential formulation.

Anisotropic and example-based materials. In this work we demonstrate properties of micropolar materials that enable more (artistic) control over elastic bodies than traditional isotropic materials. Therefore, we briefly discuss approaches in classic elasticity with similar goals. For example, Li and Barbic [2014] introduced stability criteria to select parameters for orthotropic materials with different stiffness parameters in three orthogonal directions. Xu et al. [2015] introduced a method to design nonlinear orthotropic materials by editing stress-strain curves. More recently, Kim et al. [2019] proposed an inversion-safe transverse isotropic material which can be used to strengthen or

soften isotropic materials in a specific fiber direction. Nevertheless, these approaches only give explicit control over shear and stretch stiffness of a material.

A different category of established methods that give users more control over physically plausible deformations is given by example-based materials [Fröhlich and Botsch 2011; Schumacher et al. 2012]. These methods require a set of example poses of a mesh and then perform a physically-based inter- or extrapolation to new configurations. However current example-based methods are based on classic elasticity and the concept is in general orthogonal to using a micropolar material model for the physical simulation.

3 A MICROPOLAR MATERIAL MODEL

Our goal is to formulate a strain energy density function which we can later minimize in an incremental potential context. To this end, we briefly review the concept of micropolar materials in Section 3.1, then define the corresponding kinematic relations and strain measures in Section 3.2. Using these strain measures, we introduce a micropolar strain energy density in Section 3.3 and discuss its properties.

Definitions and notation. Let $\boldsymbol{e}_i$ be the orthogonal unit vectors in the three coordinate directions $i = 1, 2, 3$, and we employ the Einstein summation conventions. As a shorthand for differentiation, we define

$$f_{,i} := \frac{\partial f}{\partial \boldsymbol{X}_i}, \tag{1}$$

which has the same dimensions as f. We will use superscript indices to denote running indices (e.g., nodal indices) in expressions where it helps to avoid confusion with spatial indices.

For every vector $\boldsymbol{w} \in \mathbb{R}^3$ there exists a cross product matrix $\text{cross}(\boldsymbol{w}) \in \mathbb{R}^{3\times3}$ such that $\text{cross}(\boldsymbol{w})\boldsymbol{v} = \boldsymbol{w} \times \boldsymbol{v}$ for any $\boldsymbol{v} \in \mathbb{R}^3$. Given a skew-symmetric matrix $\mathbf{W}$, we denote the unique vector $\boldsymbol{w} \in \mathbb{R}^3$ such that $\mathbf{W} = \text{cross}(\boldsymbol{w})$ by $\text{axl}(\mathbf{W})$. We will denote the symmetric part of a matrix by $\text{sym}(\mathbf{A})$ and the skew-symmetric part $\text{skew}(\mathbf{A})$.

We assume the reader is familiar with the basics of classic elasticity and refer to the course notes of Kim and Eberle [2022] and Sifakis and Barbic [2012] for an introduction to this field. In the following we will present a total Lagrangian formulation, i.e. a material model with respect to a fixed reference (material) configuration $\Omega \subset \mathbb{R}^3$ where uppercase $\boldsymbol{X} \in \Omega$ denotes material points in the reference configuration and lowercase $x(\boldsymbol{X})$ are the corresponding positions in the deformed configuration.

3.1 Micropolar continua

Micropolar materials are a special case of more general *micromorphic materials* [Eringen 1999]. In addition to the displacement, micromorphic materials exhibit a "microstructure" that can, depending on the specific class of material rotate, stretch and possibly shear independently from its macroscopic (classic) deformation. In three-dimensional space the microstructure can be described by a set of three "directors" $\{\boldsymbol{d}_1, \boldsymbol{d}_2, \boldsymbol{d}_3\} \in \mathbb{R}^3$ in each material point. The directors are essentially basis vectors that usually coincide with the unit vectors $\boldsymbol{e}_i$ in the rest configuration but can change their orientation and length under internal and external forces. For micropolar materials, the directors form a rigid coordinate system attached to each material point, and the directors can be interpreted as columns of a rotation matrix $\overline{\mathbf{R}} = \boldsymbol{d}_i \otimes \boldsymbol{e}_i$. See Figure 2 for a visualization. The notation of directors and rotation matrices can be used interchangeably and we introduce it here for easier reference with related work. To summarize, in classic elasticity every material point has 3 degrees of freedom that describe its displacement from its rest position $\boldsymbol{u}(\boldsymbol{X}) : \Omega \to \mathbb{R}^3$. Micropolar materials feature

additional degrees of freedom to represent the rotation of their microstructure, the *microrotation field* $\overline{\mathbf{R}}(\boldsymbol{X}) : \Omega \rightarrow SO(3)$, where $SO(3)$ is the group of rotations in three-dimensional space.

In general, the microrotation $\overline{\mathbf{R}}$ does not coincide with the macroscopic or geometric rotation of the material $\mathbf{R}$, where the latter can be determined *uniquely* from the polar decomposition of the deformation gradient $\mathbf{F} = \mathbf{RU}$. Instead, the microrotation $\overline{\mathbf{R}}$ is an *independent* set of degrees of freedom that can be *coupled* to the material displacement depending on the specific choice of material model. Requiring that the microrotation matches the macrorotation exactly, i.e. $\overline{\mathbf{R}} = \mathbf{R}$ leads to "couple-stress" theory or higher-order gradient continuum theory which involve second and possibly higher-order derivatives of the displacement field [Grbčić et al. 2018; Sansour and Wagner 2003]. For a general discussion on the relation of these theories we refer to Steinmann and Stein [1997]. In the context of our simulations, we will discuss the coupling of the rotations in the following sections and revisit it in the evaluation in Section 5.1.

3.2 Kinematic relations

While strain measures such as the small strain tensor $\boldsymbol{\varepsilon}$ or the Green strain tensor $\mathbf{E}$ are well-known in physically-based animation, these are not sufficient for micropolar materials. We follow the formulations employed by Eremeyev et al. [2012, Chapter 4.2.1][1], which we summarize in the following. We will initially represent the microrotations $\overline{\mathbf{R}}$ as rotation matrices, but will later revisit the topic of rotational representation . We start with the deformation gradient

$$\mathbf{F} = \frac{\partial \boldsymbol{x}}{\partial \boldsymbol{X}} = \boldsymbol{x}_{,i} \otimes \boldsymbol{e}_i . \tag{2}$$

In analogy to the stretch tensor $\mathbf{U}$ from the polar decomposition of the deformation gradient $\mathbf{F} = \mathbf{RU}$, we define the (generally) *non-symmetric* stretch tensor

$$\overline{\mathbf{U}} = \overline{\mathbf{R}}^T \mathbf{F} . \tag{3}$$

While the polar factor $\mathbf{U}$ is unique for a given $\mathbf{F}$ and always symmetric positive semi-definite, this does not hold for $\overline{\mathbf{U}}$ in general as it depends on the independent variable $\overline{\mathbf{R}}$. Based on this stretch tensor we define the strain measure for stretch

$$\overline{\mathbf{E}} = \overline{\mathbf{U}} - \mathbf{I} , \tag{4}$$

which vanishes in the rest configuration and is our counterpart of the small strain tensor $\boldsymbol{\varepsilon}$ or the corotational strain tensor $\mathbf{U} - \mathbf{I}$.

While the stretch tensor $\overline{\mathbf{E}}$ measures the strain in the material due to spatially varying displacements, we need a separate strain measure for spatially varying microrotations $\overline{\mathbf{R}}$ or the *microstructure curvature*. Many alternative formulations of these curvature measures can be found in the literature, but they are usually derived from the third-order Lagrangian curvature tensor

$$\mathcal{K} = \overline{\mathbf{R}}^T \nabla \overline{\mathbf{R}} = (\overline{\mathbf{R}}^T \overline{\mathbf{R}}_{,k}) \otimes \boldsymbol{e}_k \quad \text{or} \quad \mathcal{K}_{ijk} = \overline{\mathbf{R}}_{li} \overline{\mathbf{R}}_{lj,k} . \tag{5}$$

It can be shown that each individual term $\overline{\mathbf{R}}^T \overline{\mathbf{R}}_{,k}$ is skew-symmetric which implies that $\mathcal{K}$ has only 9 independent components and can therefore be represented by a single 3×3 matrix instead. This enables us to define a matrix-valued curvature measure which is more intuitive to handle. One such option is the *wryness tensor*

$$\boldsymbol{\Gamma} = \mathrm{axl}(\overline{\mathbf{R}}^T \overline{\mathbf{R}}_{,k}) \otimes \boldsymbol{e}_k , \tag{6}$$

which will be our strain measure for curvature in the following.

[1] We refer to Neff et al. [2015] for a more straightforward introduction of the formulations introduced by Eremeyev et al. [2012] without detailed derivations. Also, several alternative definitions of strain measures can be found in the mechanics literature and we refer to Pietraszkiewicz and Eremeyev [2009] for reference.

Connection to Cosserat rods and the Darboux vector. To set the wryness tensor $\boldsymbol{\Gamma}$ in context with established formulations of one-dimensional rods, it can also be expressed in terms of the previously introduced directors $\boldsymbol{d}_i$ (i.e. the columns of $\overline{\mathbf{R}}$) as

$$\boldsymbol{\Gamma} = \frac{1}{2}\overline{\mathbf{R}}^T \underbrace{(\boldsymbol{d}_j \times \boldsymbol{d}_{j,i})}_{=:2\boldsymbol{w}_i} \otimes \boldsymbol{e}_i = \overline{\mathbf{R}}^T \boldsymbol{w}_i \otimes \boldsymbol{e}_i \tag{7}$$

which corresponds to the formulation used by Tambača and Velčić [2010]. Comparing this with the bending and twisting measure used by Kugelstadt and Schömer [2016] for the simulation of Cosserat rods, we can see that for $i = 1$ the term

$$\boldsymbol{w}_1 = \frac{1}{2}\boldsymbol{d}_j \times \frac{\partial \boldsymbol{d}_j}{\partial \boldsymbol{X}_1} \tag{8}$$

corresponds to the *Darboux* vector that describes the spatial rate of change in material orientation along a rod's centerline. Thus the wryness tensor $\boldsymbol{\Gamma}$ is a direct generalization of this concept to volumetric bodies, which allows us to interpret the entries of $\boldsymbol{\Gamma}$. An entry $\boldsymbol{\Gamma}_{ij}$ describes how the rotation around the material's i-th axis changes along its j-th axis. Therefore, the diagonal entries represent the amount of torsion around the corresponding axis while off-diagonal entries describe the amount of bending of the microstructure.

Rest curvature. While prescribing an absolute orientation as "rest rotation" is possible by considering the relative rotation $\overline{\mathbf{R}}_0^T\overline{\mathbf{R}}$ instead of $\overline{\mathbf{R}}$ everywhere, this basically changes only the directions used to measure curvature such as torsion or bending. Much more interesting for the application in physically-based animation is the possibility to prescribe a rest curvature of the material. This can be incorporated by setting

$$\overline{\boldsymbol{\Gamma}} = \boldsymbol{\Gamma} - \boldsymbol{\Gamma}_0\,, \tag{9}$$

where $\boldsymbol{\Gamma}_0$ is the rest curvature in the material frame. Minimizing a strain energy based on this modified curvature measure can then lead to internal stresses and cause deformation originating from the interior of the material depending on the choice of stiffness parameters. We will explore useful applications of the rest curvature term in the context of physically-based animation in our experiments presented in Section 5.3.

3.3 Constitutive laws

The previously introduced strain measure for stretch $\overline{\mathbf{E}}(\overline{\mathbf{R}}, \mathbf{F})$ and the wryness tensor $\boldsymbol{\Gamma}(\overline{\mathbf{R}}, \overline{\mathbf{R}}_{,k})$ as strain measure for curvature can be used to define a material model in terms of a strain energy density function Ψ which we will assume to be the sum of two separable terms

$$\Psi(\overline{\mathbf{E}}, \overline{\boldsymbol{\Gamma}}) = \Psi_{\text{mp}}(\overline{\mathbf{E}}) + \Psi_{\text{curv}}(\overline{\boldsymbol{\Gamma}})\,. \tag{10}$$

Note that Ψ_{mp} and Ψ_{curv} are still coupled through the dependence on the microrotation $\overline{\mathbf{R}}$. We will refer to Ψ_{mp} as the micropolar strain energy density and to Ψ_{curv} as the micropolar curvature energy density.

3.3.1 A "physically linear" micropolar material. In computer graphics, nonlinear material models are quite common as they are usually trivially invariant to rigid rotations and are able to model (near) incompressibility better. While fully nonlinear micropolar models exist, their use is not widespread. We will briefly discuss some nonlinear variants in Section 3.3.3. With this work, instead, we want to focus on the so-called *physically linear* micropolar materials which have in common that the corresponding stress tensor is linear in the stretch tensor $\overline{\mathbf{U}}$. However, the overall elastic problem will remain nonlinear (referred to as "geometrically nonlinear") due to the multiplicative coupling

with the microrotations $\overline{\mathbf{R}}$ as well as the nonlinear structure of $SO(3)$ itself. This makes these micropolar materials suitable for large deformations in contrast to classic linear elasticity. Here, we follow the definitions of Neff [2006] by introducing the isotropic energy densities

$$\Psi_{\text{mp,lin}}(\overline{\mathbf{E}}) = \mu\|\operatorname{sym}\overline{\mathbf{E}}\|_F^2 + \mu_c\|\operatorname{skew}\overline{\mathbf{E}}\|_F^2 + \frac{\lambda}{2}\operatorname{tr}(\overline{\mathbf{E}})^2\,, \tag{11}$$

$$\Psi_{\text{curv,iso}}(\overline{\mathbf{\Gamma}}) = \mu\frac{L_c^2}{2}(\alpha\|\operatorname{sym}\overline{\mathbf{\Gamma}}\|_F^2 + \beta\|\operatorname{skew}\overline{\mathbf{\Gamma}}\|_F^2 + \gamma\operatorname{tr}(\overline{\mathbf{\Gamma}})^2)\,, \tag{12}$$

where λ and μ are the standard Lamé parameters, μ_c is the *Cosserat couple modulus*, L_c is a characteristic length scale of the microstructure and α, β and γ are additional micropolar curvature stiffness parameters[2]. The parameters α and β are intended to control bending while γ controls stiffness to torsion. By multiplying the degrees of freedom by an arbitrary rotation matrix, it can be shown that these energies are still invariant under external rigid rotations. We will now provide some intuition for this material model.

In relation to classic hyperelasticity. First of all we want to highlight the superficial similarity of the linear micropolar strain energy $\Psi_{\text{mp,lin}}$ to common classic hyperelastic materials. The strain in classic elasticity is assumed to be symmetric and therefore the skew-symmetric part of a classic strain measure will be zero (i.e. the second term in Eq. (11) vanishes). So, if we evaluate $\Psi_{\text{mp,lin}}$ instead of $\overline{\mathbf{E}}$ with the classic small strain tensor $\boldsymbol{\epsilon}$, the corotational strain $\mathbf{R}^T\mathbf{F} - \mathbf{I}$ or the Green strain tensor $\mathbf{E}$, we actually obtain the strain energy density for linear elasticity, corotated linear elasticity and the St. Venant Kirchhoff model, respectively.

For micropolar materials, the strain measure $\overline{\mathbf{E}}$ can be asymmetric and in consequence the stress tensors resulting from the internal energy densities are generally asymmetric as well. This can be used to model internal torques or "couple-stresses" as well as the application of torsional loads directly in the interior (or on the surface) of the material [Dadgar-Rad and Hossain 2023].

The couple modulus μ_c. Introduced as a new material parameter, the Cosserat couple modulus μ_c can be roughly interpreted as the stiffness of a constraint coupling the microrotation field $\overline{\mathbf{R}}$ to the geometric or macrorotation $\mathbf{R}$ of the deformation gradient [Fischle and Neff 2017b; Münch 2007]. In this context we can highlight a few special cases.

Setting $\mu_c = 0$ the coupling to the macrorotations vanishes completely. The microrotation field will only be determined through boundary conditions and the formulation of the curvature energy density Ψ_{curv}. However, the resulting microrotation field will still have an influence on the stresses in the material through the strain measure $\overline{\mathbf{E}}$. In combination with the fully physically linear strain energy density $\Psi_{\text{mp,lin}}$, this can lead to similar effects as classic linear elasticity under large rotations.

For values $\mu_c \geq \mu$ the microrotations become more strongly coupled to the macrorotations. Ignoring external loads (body forces and boundary conditions) and considering a micropolar length scale of $L_c = 0$ (i.e. zero curvature energy), Fischle and Neff [2017a] have shown that the polar factor $\mathbf{R}$ is actually the unique minimizer of the Cosserat shear-stretch energy terms from Eq. (11)

$$\mu\|\operatorname{sym}(\overline{\mathbf{R}}^T\mathbf{F} - \mathbf{I})\|_F^2 + \mu_c\|\operatorname{skew}(\overline{\mathbf{R}}^T\mathbf{F} - \mathbf{I})\|_F^2 \tag{13}$$

[2]For the strain energy $\Psi_{\text{mp,lin}}$ different expressions can be found in the literature. The representation introduced by Eringen [1999] which is also commonly used (see e.g. [Eremeyev et al. 2012, Chapter 4.6],[Ramezani et al. 2009]) can be shown to be equivalent by appropriate conversion of the material parameters (see [Münch 2007, Appendix A.6]).

For the curvature energy $\Psi_{\text{curv,iso}}$ we set the parameter α_4 of the original expression proposed by Neff [2006] to zero for simplicity as it did not have considerable influence in our experiments.

for a given $\mathbf{F}$. Moving towards $\mu_c \to \infty$ increases the strength of the coupling and ultimately leads to the aforementioned limit case of "couple-stress theory" where the rotation degrees of freedom are directly dependent on the displacement field which requires specialized numerical treatment.

When applying the physically linear material model in the context of physically-based animation, our goal is to indeed have some degree of coupling between the micro- and macrorotations as this allows us to influence the material deformation using the micropolar curvature energy in a controlled way. Therefore, we suggest a choice of $\mu_c \approx \mu$ as we want to avoid artifacts from rotations deviating too far from the macrorotations ($\mu_c \ll \mu$) as well as possible locking due to the lack of higher-order deformation gradient information when using linear discretizations ($\mu_c \gg \mu$).

Inspired by corotated linear elasticity which is widely used in physically-based animation (see e.g. [Kugelstadt et al. 2018; McAdams et al. 2011; Stomakhin et al. 2012]) one can also imagine a coupling term similiar to $\overline{\mathbf{R}}^T\mathbf{R} - \mathbf{I}$, where $\mathbf{R}(\mathbf{F})$ is given by the polar decomposition. In the mechanics literature only few works follow this approach (see e.g. [Böhmer et al. 2016]) and while it complicates the formulations of first- and second-order derivatives, Neff et al. [2015] also note that this would introduce a non-convex energy to the system. We therefore continue to use the more established physically linear material and leave further investigation of different coupling terms for future work.

3.3.2 Orthotropic curvature energy. The curvature energy introduced in Eq. (12) is an isotropic model and therefore does not distinguish between bending or torsion along different axes. For applications in physically-based animation, however, we can think of many scenarios where more control depending on the direction of the bending would be preferable. Consider for examples materials inspired by, e.g., cloth with directional fibers or materials that have a microstructure with holes which are not resolved by the model geometry. As part of our contribution we propose an orthotropic curvature energy that can be used instead of the isotropic curvature energy given by

$$\Psi_{\text{curv,ortho}}(\overline{\mathbf{\Gamma}}) = \mu L_c^2 \mathbf{C}_{ij} \overline{\mathbf{\Gamma}}_{ij}^{\ 2}, \tag{14}$$

where $\mathbf{C} \in \mathbb{R}^{3\times3}_+$ is a matrix of bending and torsion stiffness parameters. The entries of $\mathbf{C}$ follow the same intuition as introduced for the wryness tensor $\overline{\mathbf{\Gamma}}$, i.e. an entry $\mathbf{C}_{ij}$ defines the stiffness against a change in rotation around the i-th axis while moving in direction of the j-th axis. For anisotropic behavior which is not aligned with the unit vectors $\boldsymbol{e}_i$ in material coordinates (e.g. fibers in cross direction), it is possible to transform the curvature measure into a different basis similar to orthotropic materials in classic elasticity (see e.g. [Li and Barbic 2014]). We show application examples involving this anisotropic curvature energy in Section 5.2.

3.3.3 Fully nonlinear material models. While our experiments continue to focus on the physically linear micropolar material presented in Section 3.3.1, for completeness we will briefly discuss nonlinear variants.

The volume term

$$\frac{\lambda}{2}\operatorname{tr}(\overline{\mathbf{E}})^2 = \frac{\lambda}{2}\operatorname{tr}(\overline{\mathbf{U}} - \mathbf{I})^2, \tag{15}$$

from the micropolar strain energy density in Eq. (11) is structurally similar to the corotational volume term $\operatorname{tr}(\mathbf{U} - \mathbf{I})$ which corresponds to a linearization (see e.g. [Smith et al. 2018]) of the Neo-Hookean volume term $\ln(\det \mathbf{F})$. In addition to being a linearization, this term actually couples rigid rotational and volumetric deformation when $\overline{\mathbf{R}} \neq \mathbf{R}$. This coupling seems nonphysical and it was proposed (e.g. see [Münch 2007, Chapter 4.6] or [Fischle and Neff 2017b; Münch et al. 2011]) to replace it with a nonlinear term based on $\det \overline{\mathbf{U}} = \det(\overline{\mathbf{R}}^T\mathbf{F}) = \det \mathbf{F}$ which measures the actual

volume change. However, we noticed that combining this term with the physically linear micropolar energy can cause locking under extreme deformations and large Poisson's ratios.

Alternatively, one can consider fully nonlinear micropolar models. Ramezani et al. [2009] derived micropolar generalizations of classic nonlinear materials and based on this Bauer et al. [2012] suggested a micropolar Neo-Hookean strain energy which can be rewritten[3] as

$$\Psi_{\text{mp,NH}} = \frac{\mu}{2}(\text{tr}(\mathbf{F}^T\mathbf{F}) - 3) + \frac{\lambda}{4}(J^2 - 1) - \left(\frac{\lambda}{2} + \mu\right)\ln J + \mu_c \|\text{skew}\,\overline{\mathbf{U}}\|^2 . \tag{16}$$

This model is a variant of a classic Neohookean strain energy density augmented by the micropolar rotation coupling term that is also present in the physically linear model (as $\text{skew}\,\overline{\mathbf{U}} = \text{skew}\,\overline{\mathbf{E}}$). We performed experiments with this model in scenarios with strong twisting over multiple revolutions. However, when reaching points where linear materials would start to invert, the strong internal stresses of the Neohookean material seem to overpower and "disable" the rotation coupling term which leads to a decoupled solution of the rotation field. In this sense its strong nonlinearity does not appear to be a good fit for the micropolar coupling term and we do not see a significant advantage of such a model for the application in physically-based animation without further modifications to e.g. the coupling term.

4 DISCRETIZATION

In the following, we present an incremental potential formulation for time integration (Section 4.1) and a novel FEM spatial discretization (Section 4.2). The rotational degrees of freedom pose challenges for the application of typical methods and we discuss the necessary considerations to obtain a consistent discretization. We will later evaluate the accuracy of our discretization in Section 5.1.

Equations of motion for micropolar media. In contrast to a majority of works in the mechanics literature on micropolar media, in physically-based animation we are mainly interested in dynamic problems. While we will subsequently follow a variational approach that is not directly based on the equations of motion, let us first introduce them for reference. Following Eremeyev et al. [2012, Chapter 3.6], the momentum and angular momentum balances governing the dynamics of a micropolar continuum are given by

$$\rho_0 \dot{\boldsymbol{v}} = \boldsymbol{f}_{\text{int}} + \rho_0 \boldsymbol{g} \quad \text{and} \quad j_0 \dot{\boldsymbol{\omega}} = \boldsymbol{t}_{\text{int}} + \rho_0 \boldsymbol{m}\,, \tag{17}$$

where $\boldsymbol{v}$ and $\boldsymbol{\omega}$ are the material's linear and angular velocities, $\boldsymbol{f}_{\text{int}}$ and $\boldsymbol{t}_{\text{int}}$ are the internal forces and torques, $\boldsymbol{g}$ and $\boldsymbol{m}$ are external body linear and angular accelerations, ρ_0 is the rest density and j_0 is the scalar measure of "rotary inertia" of the microstructure in the rest configuration. The case of $j_0 = 0$ is a valid choice and results in microrotations that instantaneously align according to the balance of angular momentum.

4.1 Incremental potential formulation

Formulating implicit time integrators like Backward Euler as optimization problems is an established solution strategy that enables the use of robust optimizers and facilitates coupling of physical systems.Therefore, we do not discretize the momentum balances directly as is customary in the mechanics literature. Instead, we propose a new incremental potential formulation for micropolar elasticity. After performing a spatial and temporal discretization that we will introduce in the next sections, we arrive at an incremental potential posed in terms of velocity degrees of freedom which

[3]Note that we set $\kappa := 2\mu_c$ compared to the formulation used by Bauer et al. [2012] in order to scale it consistently with our physically linear model.

can be written as

$$\begin{aligned} E(\boldsymbol{v}, \boldsymbol{\omega}) =& \frac{1}{2}(\boldsymbol{v} - \boldsymbol{v}_0)^T \mathbf{M}_{\rho_0}(\boldsymbol{v} - \boldsymbol{v}_0) \\ &+ \frac{1}{2}(\boldsymbol{\omega} - \boldsymbol{\omega}_0)^T \mathbf{M}_{j_0}(\boldsymbol{\omega} - \boldsymbol{\omega}_0) \\ &+ E_{\text{int}} + E_{\text{ext}}\,, \end{aligned} \tag{18}$$

where $\boldsymbol{v}_0$ and $\boldsymbol{\omega}_0$ are the global velocity vectors of the previous timestep, $\mathbf{M}_{\rho_0}$ and $\mathbf{M}_{j_0}$ are the global mass and rotary inertia matrices (lumped or computed in standard FEM fashion), E_{int} is the total internal (strain) energy and E_{ext} is the potential due to external accelerations.

Contact energy. In this context, we can add robust contact handling to the simulation by introducing a potential contact. We employ the formulation by Li et al. [Li et al. 2020] which imposes a barrier potential energy E_c based on the unsigned distances d between triangle-point and edge-edge pairs in contact as

$$E_c(d) = \begin{cases} -k_c(d - \hat{d})^2 \ln(d/\hat{d}) & \text{if } d < \hat{d} \\ 0 & \text{if } d \geq \hat{d}, \end{cases} \tag{19}$$

where k_c is the barrier stiffness and $\hat{d}$ the distance at which the barrier is activated.

Energy minimization. Our overall problem for each timestep can then be written simply as

$$\min_{\boldsymbol{v}, \boldsymbol{\omega}} E(\boldsymbol{v}, \boldsymbol{\omega})\,, \tag{20}$$

with E given by Eq. (18), followed by updating the displacement field $\boldsymbol{x}$ and microrotation field $\overline{\mathbf{R}}$. To solve the minimization problem we use Newton's method with fully updated Hessians at each iteration. Due to the complexity of some of the involved expressions we choose to implement the local gradients and Hessians with the help of the symbolic differentiation framework SymX [Fernández-Fernández et al. 2023]. The scalar potential function E can be directly used for a standard backtracking line search to ensure a sufficient decrease in the objective leading to improved convergence.

4.2 FEM Discretization

For accurate results that are consistent under refinement we choose to perform the spatial discretization of the energy minimization problem using the Finite Element Method (FEM). Central to FEM is the best-approximation of a solution in the continuous domain (e.g. the displacement field $\boldsymbol{u}(\boldsymbol{X})$ in classic elasticity) in a discrete subspace. In practice this is done by dividing the solution domain into N_{el} elements T_i that each contain a set of nodal basis functions ϕ_j. The discrete solution $\boldsymbol{u}_h$ can then be expressed as a linear combination of the nodal basis functions with coefficients given by the nodal degrees of freedom $\boldsymbol{u}_j$, e.g.:

$$\boldsymbol{u}_h(\boldsymbol{X}) = \phi_j(\boldsymbol{X})\boldsymbol{u}_j\,. \tag{21}$$

This enables us to evaluate or interpolate the solution at any point in the domain. We now apply this approach to discretize our internal energy of the micropolar continuum given by

$$E_{\text{int}} = \int_\Omega \Psi(\boldsymbol{X}) d\boldsymbol{X} \approx \sum_i^{N_e} \int_{T_i} \Psi(\boldsymbol{X}) d\boldsymbol{X}\,, \tag{22}$$

where we use $\Psi(\boldsymbol{X})$ as a shorthand implying the evaluation of the strain measures $\overline{\mathbf{E}}$ and $\overline{\boldsymbol{\Gamma}}$ at point $\boldsymbol{X}$. To evaluate the element-wise integrals we transform the integral to a reference element $\hat{T}$ where

we apply a quadrature rule for numerical integration

$$\sum_i^{N_e} \int_{T_i} \Psi(\boldsymbol{X}) d\boldsymbol{X} = \sum_i^{N_{\text{el}}} \int_{\hat{T}} \Psi(\boldsymbol{\xi}_i(\hat{\boldsymbol{X}})) |\det(\mathbf{J}_i(\hat{\boldsymbol{X}}))| d\hat{\boldsymbol{X}} \tag{23a}$$

$$\approx \sum_i^{N_{\text{el}}} \sum_j^{N_{\text{qp}}} w_j \hat{\Psi}(\hat{\boldsymbol{p}}_j) |\det(\mathbf{J}_i(\hat{\boldsymbol{p}}_j))|\,, \tag{23b}$$

where quantities with a hat indicate quantities in the reference element $\hat{T}$, $\hat{\boldsymbol{p}}_j$ and w_j are the quadrature points and weights in the reference element, $\boldsymbol{\xi}_i : \hat{T} \rightarrow T_i$ is the mapping from the reference element to the corresponding element T_i in material coordinates and $\mathbf{J}_i$ is the Jacobian of this mapping.

As can be seen in Eq. (23b), in practice we have to interpolate our degrees of freedom to the quadrature points in the reference element. While this is trivial for the displacement field as shown in Eq. (21), this is not directly applicable to the microrotation field $\overline{\mathbf{R}}$ which we need for both of the micropolar strain measures $\overline{\mathbf{E}}$ and $\overline{\boldsymbol{\Gamma}}$ to evaluate the corresponding energy contributions.

4.2.1 Discretizing the microrotation field. Common rotation representations like rotation matrices or unit quaternions do not form a vector space and so a linear combination of them as part of FEM might not result in a proper rotation. Therefore, we avoid interpolating rotations with a naive linear combination. Before we introduce our formulation, let us first briefly discuss alternatives suggested in the literature.

Previous approaches. An approach commonly found in the mechanics literature (see e.g. [Bauer et al. 2010; Münch 2007; Sansour and Wagner 2003]) is based on the linear combination of rotation vectors (also known as Euler vectors) which represent a rotation as a vector $\boldsymbol{\Theta} = \theta \boldsymbol{n} \in \mathbb{R}^3$ where θ is the angle of rotation and $\boldsymbol{n}$ the normalized axis of rotation. This corresponds to interpolation in the tangent space of the identity rotation. However, interpolating large rotations far away from the identity rotation in this way can lead to "distorted" results and the mapping between representations introduces singularities that have to be considered.

A generalized concept of interpolation that actually respects the nonlinearity of $SO(3)$ can be defined using the Riemannian weighted center of mass and a respective distance metric [Moakher 2002]. In our context this would result in nonlinear optimization problems locally in each element which can be solved iteratively, e.g., using the "Spherical Weighted Averages" algorithm proposed by Buss and Fillmore [2001]. Except for special cases however, no closed form solution for more than two rotations (which corresponds to spherical linear interpolation) exists. For implicit time integration this poses problems as differentiation of this procedure is practically only possibly using algorithmic differentiation.

As discussed in related work, we consider the Geodesic FEM framework introduced by Sander [2012] to be too complex and not computationally efficient enough for direct application in the context of physically-based animation, and we pursue an alternate approach instead.

Quaternion linear blending. In QLB, rotations are blended by computing a linear combination of a set of unit quaternions followed by renormalization [Kavan and Žára 2005]. While the method appears to be well suited for e.g. skinning in practice, a few theoretical considerations make it slightly less attractive for use in FEM. Error bounds for the interpolation between two quaternions were presented but the situation is unclear for more than two. Furthermore, the given analysis of the error bounds assumes a maximum angle between the vector representations below 90 degrees. This can be trivially ensured in case of two quaternions by flipping one of their signs. However, for

more than two quaternions this requirement can only be satisfied with respect to one of them, not between all pairs. Similar to the approach of interpolating rotation vectors, these considerations are related to directly interpolating possibly large rotations far away from the identity rotation.

We expect these problems to be much less relevant in practice for a method that instead either works with incremental rotations with respect to the previous timestep or with angular velocities. While we propose an approach based on angular velocities in the following, we note that it would be interesting to investigate the feasibility and accuracy of a system based on position-level DOFs when interpolating (possibly incremental) quaternions in the future.

Interpolating angular velocities. In contrast to the previously mentioned methods, we propose the following scheme for the discretization of the micropolar rotations. As already suggested by our incremental potential formulation in Section 4.1, we will continue working with velocities as degrees of freedom. Both the displacement velocity $\boldsymbol{v}$ as well as the microrotation angular velocity $\boldsymbol{\omega}$ can be linearly interpolated as elements of $\mathbb{R}^3$. This allows us to evaluate the nodal degrees of freedom ($\boldsymbol{v}_i$ and $\boldsymbol{\omega}_i$) at any point in the domain. To evaluate the involved energies in terms of the velocity DOFs, we substitute all occurrences of displacements and rotations with a corresponding time integration update rule depending on the solution of the previous timestep and the updated velocities from the current Newton iteration. For the displacement we use backward Euler for the time integration and substitute

$$\boldsymbol{u}(\boldsymbol{v}) = \boldsymbol{u}_0 + \Delta t \boldsymbol{v}\,, \tag{24}$$

where $\boldsymbol{u}_0$ is the solution of the previous timestep and $\boldsymbol{v}$ is the velocity in the current Newton step. Let $\boldsymbol{\omega}_q$ denote the purely imaginary quaternion with its coefficients given by the vector $\boldsymbol{\omega}$. For the rotation we could then employ the quaternion exponential function [Grassia 1998] to obtain

$$\boldsymbol{q}(\boldsymbol{\omega}) = \exp\left(\frac{\Delta t}{2}\boldsymbol{\omega}_q\right)\boldsymbol{q}_0\,, \tag{25}$$

which is the exact solution for a constant angular velocity over the timestep [Solà 2017]. However, we prefer the approximation

$$\boldsymbol{q}(\boldsymbol{\omega}) \approx \frac{\tilde{\boldsymbol{q}}(\boldsymbol{\omega})}{\|\tilde{\boldsymbol{q}}(\boldsymbol{\omega})\|} \quad \text{with} \quad \tilde{\boldsymbol{q}}(\boldsymbol{\omega}) = \boldsymbol{q}_0 + \frac{\Delta t}{2}\boldsymbol{\omega}_q\boldsymbol{q}_0 \tag{26}$$

as it is easier to differentiate and does not require "sinc" functions for a singularity free implementation. We implemented both variants and the error of the latter was negligible for typical timestep sizes (Δt around $10ms$).

This approach of interpolating nodal angular velocities followed by time integration is essentially equivalent to interpolating nodal incremental rotation vectors relative to the rotation of the previous timestep (in contrast to using total rotation vectors relative to the identity rotation as discussed before). This can be seen as the incremental rotation vector over a timestep Δt with constant angular velocity $\boldsymbol{\omega}$ is given directly by $\boldsymbol{\Theta} = \Delta t\boldsymbol{\omega}$ which can then be mapped to a proper rotation using the exponential map. We explicitly chose to use angular velocities here as they are anyway needed in the context of dynamic simulations.

However, at this point we did not solve the problem completely, as the quaternion update rules depend on the rotation from the previous timestep $\boldsymbol{q}_0$ at the point of evaluation (i.e. the quadrature point). While the updated displacement $\boldsymbol{u}(\boldsymbol{v})$ from Eq. (24) can be trivially evaluated everywhere in the domain because $\boldsymbol{u}_0(\boldsymbol{X})$ can be reconstructed everywhere by only keeping track of the nodal values and evaluating their FEM interpolation, this is not the case for $\boldsymbol{q}_0$. Again, because rotations do not form a vector space we cannot easily reconstruct $\boldsymbol{q}_0(\boldsymbol{X})$ from nodal values. However, as FEM only requires the evaluation at a (usually constant) set of quadrature points $\hat{p}_i$, we can solve

this by simply storing the rotations at the quadrature points $\boldsymbol{q}(\hat{\boldsymbol{p}}_i)$ over time in addition to the nodal values.

To summarize the handling of rotations in our implementation, here is an overview of the steps deviating from a standard nonlinear FEM implementation:

(1) Before simulation: initialize "old" rotations $\boldsymbol{q}_0$ at the quadrature points $\hat{\boldsymbol{p}}_i$ to be consistent with nodal initial values, e.g., $\boldsymbol{q}_0(\hat{\boldsymbol{p}}_i) \leftarrow \boldsymbol{q}_{\mathrm{id}}$.
(2) During Newton iterations: Using Eq. (26) compute the current $\boldsymbol{q}(\hat{\boldsymbol{p}}_i)$ with the stored $\boldsymbol{q}_0(\hat{\boldsymbol{p}}_i)$ and linearly interpolated current $\boldsymbol{\omega}(\hat{\boldsymbol{p}}_i)$.
(3) After Newton converged: Interpolate the converged solution $\boldsymbol{\omega}$ to quadrature points again and update $\boldsymbol{q}_0(\hat{\boldsymbol{p}}_i)$ for use in the next timestep.

There seems to be evidence that the interpolation of incremental rotations that are used to update history variables at the quadrature points can lead to an artificial path dependence of the solution [Crisfield and Jelenić 1999; Sansour and Wagner 2003]. However, in practice we did not notice any qualitative problems of this kind and we consider the accuracy gain of interpolating only small increments in contrast to possibly large total rotations to be of higher importance in the application of computer graphics. We evaluate the accuracy of this interpolation procedure in Section 5.1.

4.2.2 Evaluation of rotation gradients. In the previous section we introduced our interpolation scheme for the microrotations $\overline{\mathbf{R}}$ which we now represent using quaternions. In addition to the rotations themselves, we have to evaluate spatial gradients of the rotations in order to compute the wryness tensor $\overline{\boldsymbol{\Gamma}}$ introduced in Eq. (6) at the quadrature points.

First of all, we want to be able to compute the wryness tensor directly from the gradient of the rotation quaternions in order to avoid unnecessary conversions between representations. To do so, we generalize the formulation employed by Kugelstadt and Schömer [2016] for the rotation gradient in rods. For a quaternion $\boldsymbol{q}$, let $\mathrm{vec}(\boldsymbol{q}) \in \mathbb{R}^3$ denote the coefficients of its imaginary part and $\mathrm{conj}(\boldsymbol{q})$ denote its conjugate quaternion. Then, the wryness tensor $\overline{\boldsymbol{\Gamma}}$ can be expressed in terms of unit quaternions by

$$\overline{\boldsymbol{\Gamma}} = 2\,\mathrm{vec}(\mathrm{conj}(\boldsymbol{q})\boldsymbol{q}_{,i}) \otimes \boldsymbol{e}_i - \boldsymbol{\Gamma}_0\,. \tag{27}$$

Evaluating the spatial derivatives $\boldsymbol{q}_{,i}$ of the rotations while taking into the account the nonlinearity of Eq. (26) is quite complex. Instead, we make an approximation by evaluating them using the FEM basis gradients

$$\boldsymbol{q}_{,i} = \frac{\partial \boldsymbol{q}}{\partial \boldsymbol{X}_i} \approx \frac{\partial \hat{\phi}^k}{\partial \hat{\boldsymbol{X}}_j}\frac{\partial \hat{\boldsymbol{X}}_j}{\partial \boldsymbol{X}_i}\boldsymbol{q}^k = \left(\mathbf{J}^{-T}\frac{\partial \hat{\phi}^k}{\partial \hat{\boldsymbol{X}}}\right)_i \boldsymbol{q}^k\,, \tag{28}$$

where k denotes the summation over the nodes of an element. We evaluate the error of this approximation in Section 5.1.

4.2.3 Choice of quadrature rule. While our approach is not limited to linear elements, we follow common practice in computer graphics and use linear tetrahedral meshes in our implementation. In classic hyperelasticity, a single quadrature point is sufficient to accurately integrate any strain energy as linear elements have a constant deformation gradient. However, this does not apply to the wryness tensor $\overline{\boldsymbol{\Gamma}}$ due to the nonlinear interpolation of the rotations. Using a one point quadrature rule can lead to drifting nodal rotations and oscillating angular velocities that do not affect the overall energy of the system. Behavior like this is known in the FEM community as hourglass or zero-energy modes [Kosloff and Frazier 1978]. However, in contrast to classic elasticity, it manifests in the rotation field and not in the displacement field in our case. Over time, this can then indirectly affect the displacements due to the coupling of the fields. In the case of linear tetrahedrons this

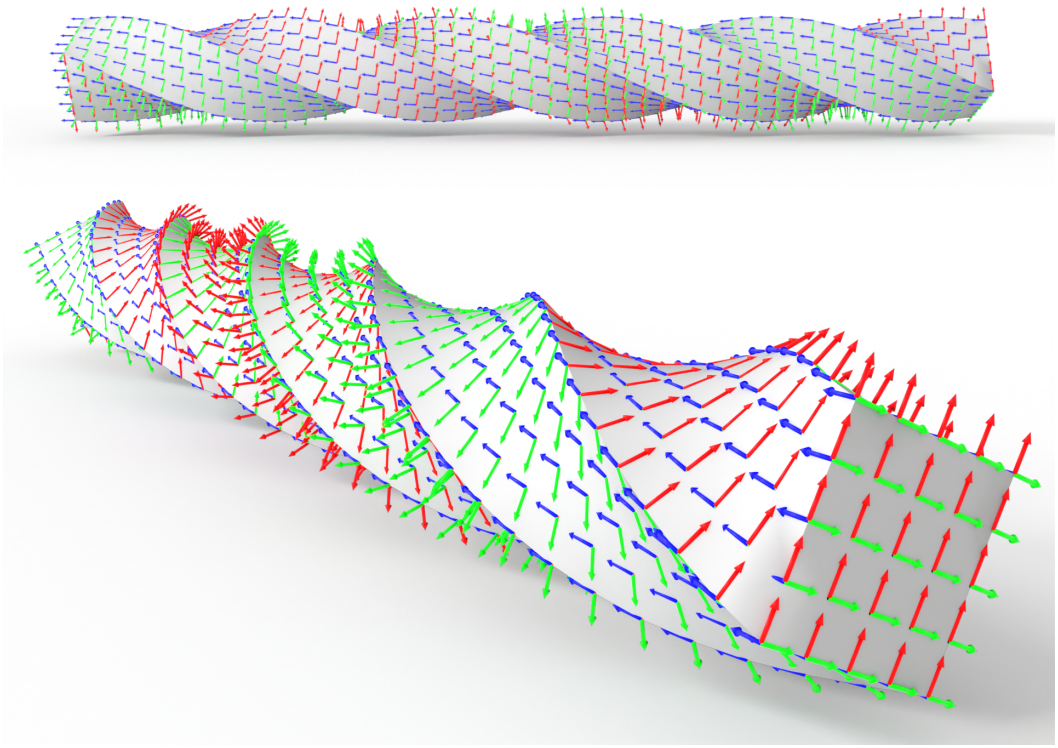

Fig. 2. Twisted cantilever for validation of our discretization. Coordinate frames visualize the microrotation field $\overline{\mathbf{R}}$ which qualitatively follows the geometric rotation.

problem was completely eliminated for all of our experiments by using a standard four point Gauss quadrature rule (see e.g. [Shunn and Ham 2012]).

5 RESULTS

In the following we validate our proposed discretization of micropolar elasticity and show examples that demonstrate its applicability in physically-based animation.

For the experiments we use a fixed gradient norm stopping tolerance of 10^{-8} for Newton's method. In each step, we solve the linear system with CG, preconditioned with a 3×3 block diagonal Jacobi preconditioner and a relative residual norm stopping tolerance of 10^{-12}. In the following, we will use the "angular distance" between two rotations as an error metric represented by the angle required to rotate one quaternion onto the other given by[4]

$$\operatorname{dist}(\boldsymbol{q}_1, \boldsymbol{q}_2) = \arccos(2(\boldsymbol{q}_1 \cdot \boldsymbol{q}_2)^2 - 1)\,. \tag{29}$$

If not specified otherwise, the microrotation field is initialized to be uniform and parallel to the global coordinate axes, i.e. the material is assumed to be "flat" in its initial configuration. We use penalty forces to apply boundary conditions in terms of target velocities and angular velocities.

[4]Note that in the originally published version of this paper Eq. (29) was erroneous. However, the results were based on the correct formula that is now shown here. The formula is based on the metric Φ_6 from Huynh [2009] using $\Phi_6 = 2\Phi_3$ [Huynh 2009, Eq. (34)] and the identity $2\arccos(|t|) = \arccos(2t^2 - 1)$.

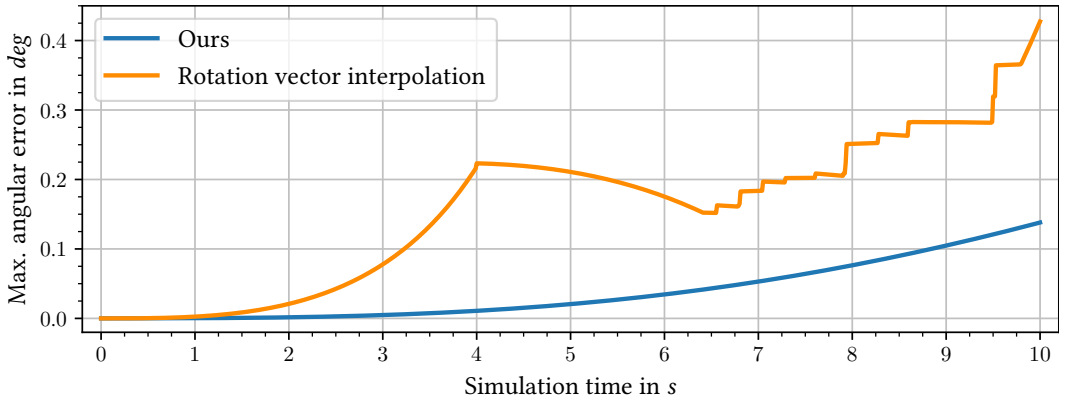

Fig. 3. Max. error of rotations at quadrature points compared to the solution obtained with spherical averaging.

5.1 Validation of our discretization

For a basic verification of our discretization, we simulate a clamped cantilever (0.05 m×0.05 m×0.6 m, $E = 1 \cdot 10^4$ Pa, $\nu = 0.3$, $\mu_c = \mu$, $L_c = 0$) that is discretized with around 9200 linear tetrahedrons in zero gravity. Both ends are rotated in opposite directions with a constant angular velocity of $\omega_{\text{BC}} = 45$ deg/s over a duration of 10 s with a timestep of $\Delta t = 10$ ms.

The state of the cantilever at the end of the last time step is shown in Fig. 2. To converge, 1-2 Newton iterations were required per timestep with 65 CG iterations on average. Over the whole mesh the maximum "twist" (angular distance) between nodal rotations within one element evaluates to 31 degrees with the given discretization. Qualitatively, the microrotation field $\overline{\mathbf{R}}$ follows the geometric deformation of the mesh. This is confirmed by an average angular distance of the microrotations $\overline{\mathbf{R}}$ to macrorotations $\mathbf{R}$ (computed using the polar decomposition of $\mathbf{F}$) of only 2.62 degrees at the end of the simulation.

To measure the accuracy of our angular velocity based interpolation approach for the microrotations (Section 4.2.1) we apply the spherical weighted averages algorithm [Buss and Fillmore 2001] to compute the microrotations at all quadrature points to high accuracy (stopping tolerance of 10^{-14}). For comparison, we also implemented an interpolation scheme based on rotation vectors with handling for large rotations as described by Münch [2007, Chapter 2.5]. The angular distance of the two interpolation schemes versus the reference solution is shown in Fig. 3. We can see that our angular velocity based interpolation yields more accurate results over the whole simulation. For much longer simulations than shown here, it would be possible to even further reduce the error by regularly "resetting" the quadrature point microrotations between timesteps using results obtained from spherical blending.

Applying algorithmic differentiation with TinyAD [Schmidt et al. 2022] to the spherical weighted averages algorithm, we can also compute reference values for the rotation gradient and curvature measure $\overline{\mathbf{\Gamma}}$. In comparison to this reference solution, our curvature measure based on the FEM interpolation of the rotation gradient (Section 4.2.2) has a maximum relative error of only 0.8% at the end of the simulation.

Overall, we conclude that our discretization appears to correctly handle large rotations of more than 360 degrees and in particular our angular velocity based interpolation approach achieves an even smaller error than the prevalent interpolation scheme based on rotation vectors.

5.2 Bending and torsion stiffness

In this section we demonstrate the enhanced level of control that micropolar materials can provide in comparison to classic materials, especially in terms of their ability to impose anisotropic bending and torsion stiffness in addition to stretching and shearing.

5.2.1 Stretchy sheet. Figure 1 (left) shows a comparison between the classic Neo-Hookean material model and the micropolar material model for a clamped volumetric thin sheet colliding with a sphere. This experiment aims to simulate a deformable object that can stretch but that is stiff to bending. Classic materials can only directly model stiffness to stretching and shearing, which leads to their resistance to bending being directly imposed by the thickness of the object in conjunction with the stiffness. As a consequence, the expected material behavior is impossible to obtain. With micropolar materials we can specify stretching and bending stiffness independently, allowing us to achieve the desired effect.

5.2.2 Hollow bunny. Figures 4 and 5 demonstrate another application of micropolar materials in computer graphics, where we compare it with classic Neo-Hookean in two scenes involving complex and thin geometries. The objective is to simulate an object that is soft to stretch but retains its shape under gravity. Classic materials often require a certain stiffness to prevent collapse, resulting in a stiffer material than desired for the scene. With the added micropolar bending stiffness however, it is possible to prevent the object from collapsing, while keeping it soft and "stretchy".

5.3 Rest curvature experiments

In addition to the higher degree of control over the stress-strain relationship, micropolar materials allow for deformations induced by changing the volumetric rest pose curvature, which we will showcase in the following experiments. We can also imagine deformation related to more complex physical phenomena, such as burning, melting or wetting, could be achieved by tying the microrotation curvature to other fields such as temperature or humidity, but such experiments are out of scope for this work.

5.3.1 Helix. In this experiment we use the micropolar material in five volumetric rods to obtain a helix shape, see Fig. 6. This is achieved by scaling up a rest pose curvature around the vertical axis, which induces a circular deformation, in addition to torsion around the rods principal direction, which adds a twist that results in each road forming a helix. This experiment validates our generalization to higher dimensions as this simulation matches the expected behavior for one dimensional rods shown by Kugelstadt and Schömer [2016]. Note that, in contrast to Cosserat rods, our simulated rods are volumetric and can be stretched and compressed in directions normal to the centerline.

5.3.2 Lotus flower. Similar to the previous experiment, we induce deformations by modifying the rest microrotation field of three volumetric thin sheets to form a lotus-like shape, see Fig. 1 (right). In this case, the prescribed deformations are dependent on time and the two-dimensional median plane of the sheets which shows that our generalized solution works well for higher than one dimensionally dominated bodies.

5.3.3 Lotus bowl. Our incremental potential formulation works robustly when integrated in a standard computer graphics solver pipeline, including IPC-style contact handling (Section 4.1), as demonstrated by the simulation shown in Fig. 7. Four lotus flowers are dropped in a bowl where they collide with each other while the elastic bending resistance maintains the shape that was prescribed through the rest pose curvature.

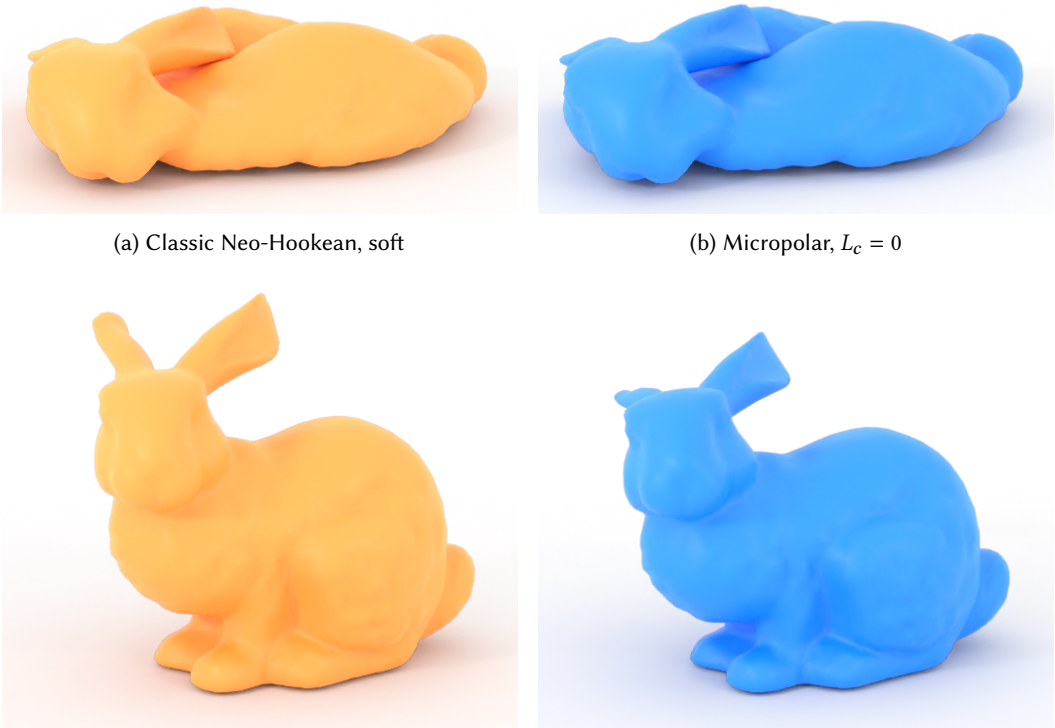

(a) Classic Neo-Hookean, soft

(b) Micropolar, $L_c = 0$

(c) Classic Neo-Hookean, stiff

(d) Micropolar, anisotropic

Fig. 4. A hollow bunny (1 m tall, 2 cm thickness) subject to gravity. With classic elasticity (left column) the bunny is either soft and collapses ($E = 5 \cdot 10^4$ Pa) or stiff and able to support its weight ($E = 2 \cdot 10^5$ Pa). With a soft micropolar material ($E = 5 \cdot 10^4$ Pa), the bunny collapses without curvature energy (top right) but with some anisotropic bending stiffness ($\mu_c = \mu$, $L_c = 1.0$, $\mathbf{C}_{yx} = \mathbf{C}_{yz} = 1$, $\mathbf{C}_{yy} = 20$) the soft material can support the weight without becoming rigid.

5.4 Two-dimensional planar shell model

To demonstrate that we can also apply micropolar materials in two dimensions with only minor modifications, we simulate an initially planar two-dimensional shell clamped on two sides under gravity as shown in Fig. 8. For the microrotations, our discretization described in Section 4.2.1 can be used without modification. The mid-plane deformation of the plate is described by the deformation gradient $\mathbf{F} \in \mathbb{R}^{3\times 2}$ which can be computed as described by Kim [2020]. The shell bending energy can be formulated in terms of the orientation of the director $\boldsymbol{d}_3$ (which is orthogonal to the plate in the rest pose) and the wryness tensor from Eq. (6) reduces to

$$\boldsymbol{\Gamma}_{\text{plate}} = \overline{\mathbf{R}}^T \left(\frac{\partial \boldsymbol{d}_3}{\partial \boldsymbol{X}_1} \otimes \boldsymbol{e}_1 + \frac{\partial \boldsymbol{d}_3}{\partial \boldsymbol{X}_2} \otimes \boldsymbol{e}_2 \right) .$$

The resulting model is a Reissner-Mindlin type plate which has a virtual thickness that introduces a resistance to shearing [Neff et al. 2010; Sander et al. 2016]. However, in contrast to the corresponding models from classic elasticity, higher-order gradients and C^1 continuity are not needed for the micropolar model. An extension to non-planar rest configurations is possible but requires a more rigorous derivation involving concepts from differential geometry, similar to the approach described

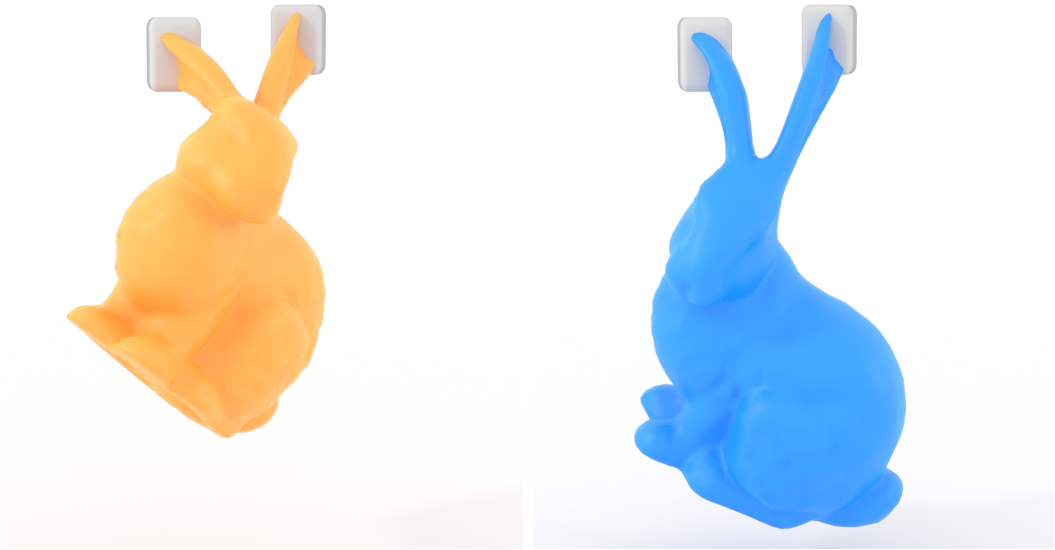

Fig. 5. We clamp the ears of the hollow bunny and remove the floor. While the bunny with the stiff Neo-Hookean (left) from Fig. 4 swings almost rigidly, the micropolar material with bending stiffness (right) that previously was able to support the bunny's weight is able to stretch and deform.

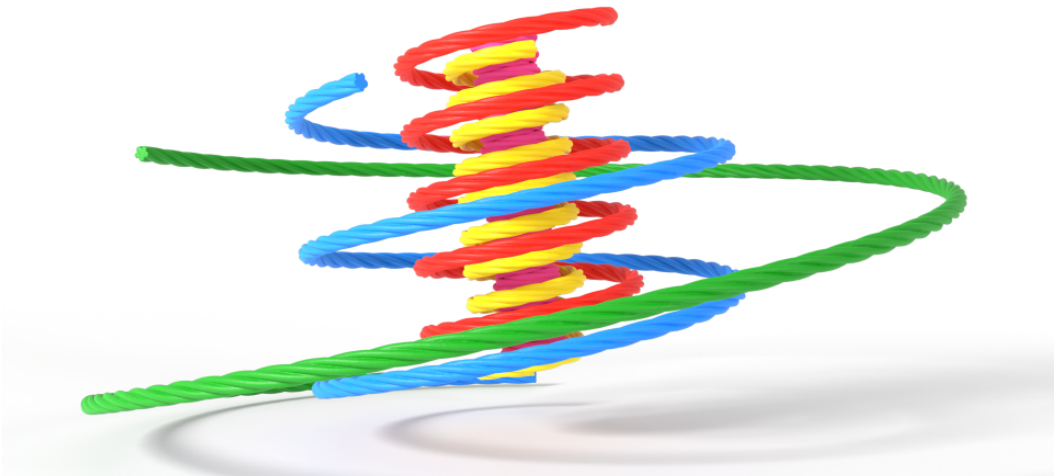

Fig. 6. Five volumetric rods with helicoidal shape are deformed by modifying their rest pose curvature over time with different intensities until they form a helix.

by Clyde et al. [2017, Supplemental] for Kirchhoff-Love shells. As with other shell models, micropolar shells can also suffer from membrane locking [Quaglino 2012], unless at least second-order elements are used for the discretization of the displacement. A common work-around in computer graphics is to combine a very soft bulk stiffness with strong strain-limiting [Li et al. 2021] which we also use for the soft case in Figure 8.

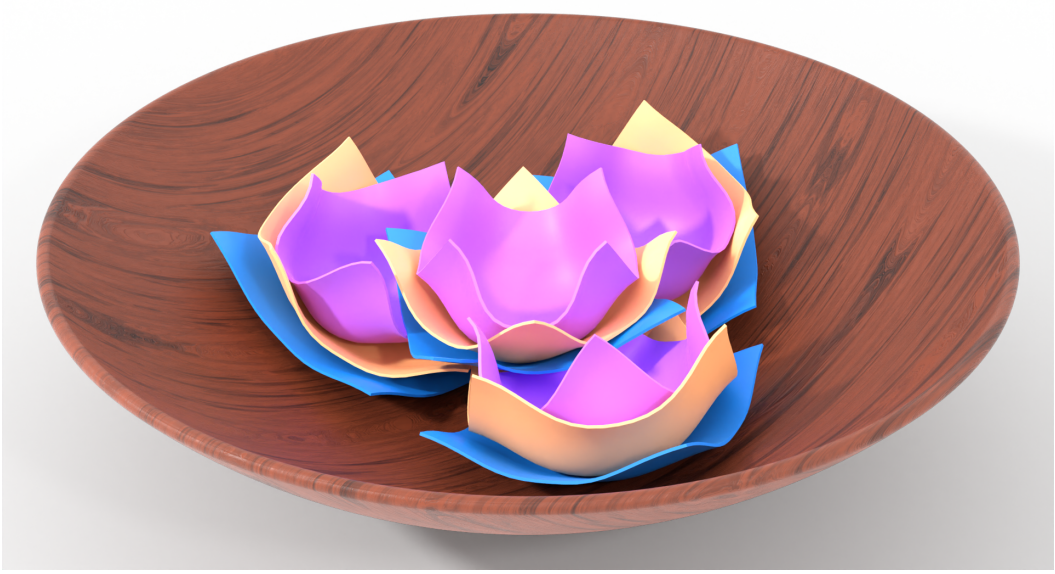

Fig. 7. Four lotus flowers are dropped into a bowl. They collide dynamically with an IPC-inspired contact model.

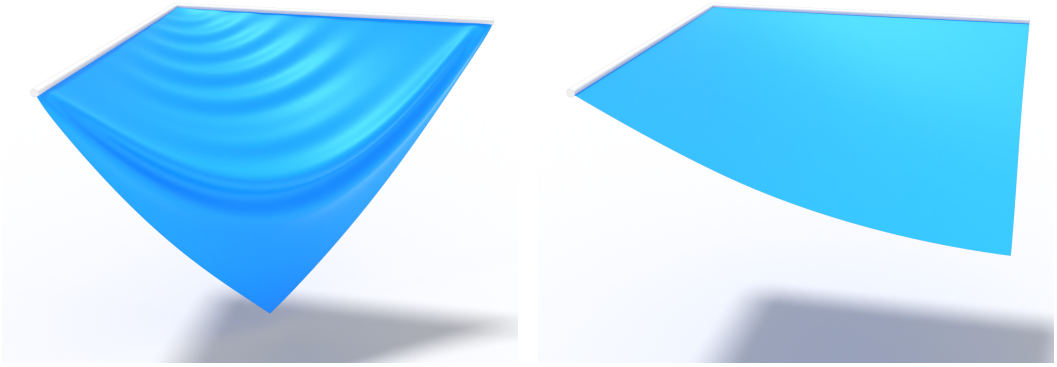

Fig. 8. A two-dimensional shell clamped on two sides under gravity. The micropolar shell model contains a continuous bending energy analogous to the three-dimensional case (left: low bending stiffness, right: higher bending stiffness).

6 CONCLUSION

In this work, we introduced two and three-dimensional micropolar materials to the physically-based animation community and proposed a consistent discretization well suited for the application in this field. We propose a FEM approach that accurately handles large rotations and integrates well with an incremental potential formulation. Our experiments showcase the extra control that micropolar materials offer in simulations that could not be achieved with classic materials, such as simulating soft materials that are stiff to bending. We also demonstrate the potential of deformations induced by changes in the rest curvature in scenes with large deformations and contacts.

In comparison to classic models, we have to solve for twice the amount of degrees of freedom which can slow down important parts of the simulation, including computation of element matrices, assembly, and global system solves. However, the impact of this difference varies depending on the scene and other effects present such as contacts and material stiffness.

Our proposed formulation is built around a backward Euler time discretization for positions and a first-order approximation for rotations. To reduce numerical damping and to take advantage of proper damping models (e.g. [Brown et al. 2018; Xu and Barbič 2017]) we would like to investigate the applicability of higher-order integration methods like BDF2 or DIRK methods [Löschner et al. 2020] in the future.

Simulation of complex and delicate materials is a very interesting path forward for micropolar models in computer graphics. While we showed creative and artistic applications for the application of micropolar materials, we believe that deformations induced by controlling the microrotation field can be useful for the simulation of complex phenomena such as wetting or burning, causing plastic deformation [Grammenoudis and Tsakmakis 2005] where the material bends and deforms in intricate ways.

ACKNOWLEDGEMENTS

We thank Theron Guo for his valuable feedback and discussions. The bunny model is courtesy of the Stanford Computer Graphics Laboratory. This work is funded by the Deutsche Forschungsgemeinschaft (DFG, German Research Foundation) — 281466253.

REFERENCES

Rafael Abreu and Stephanie Durand. 2021. Understanding Micropolar Theory in the Earth Sciences II: The Seismic Moment Tensor. *Pure and Applied Geophysics* 178, 11 (nov 2021), 4325–4343. https://doi.org/10.1007/s00024-021-02894-w

Rafael Abreu, Christine Thomas, and Stephanie Durand. 2018. Effect of observed micropolar motions on wave propagation in deep Earth minerals. *Physics of the Earth and Planetary Interiors* 276 (2018), 215–225. https://doi.org/10.1016/j.pepi.2017.04.006 Special Issue:15th SEDI conference.

Baptiste Angles, Daniel Rebain, Miles Macklin, Brian Wyvill, Loic Barthe, Jp Lewis, Javier Von Der Pahlen, Shahram Izadi, Julien Valentin, Sofien Bouaziz, and Andrea Tagliasacchi. 2019. VIPER: Volume Invariant Position-based Elastic Rods. *Proc. ACM Comput. Graph. Interact. Tech.* 2, 2, Article 19 (July 2019), 26 pages. https://doi.org/10.1145/3340260

S. Bauer, W. G. Dettmer, D. Perić, and M. Schäfer. 2012. Micropolar hyperelasticity: constitutive model, consistent linearization and simulation of 3D scale effects. *Computational Mechanics* 50, 4 (jan 2012), 383–396. https://doi.org/10.1007/s00466-012-0679-9

S. Bauer, M. Schäfer, P. Grammenoudis, and Ch. Tsakmakis. 2010. Three-dimensional finite elements for large deformation micropolar elasticity. *Computer Methods in Applied Mechanics and Engineering* 199, 41-44 (oct 2010), 2643–2654. https://doi.org/10.1016/j.cma.2010.05.002

Jan Bender, Dan Koschier, Patrick Charrier, and Daniel Weber. 2014. Position-Based Simulation of Continuous Materials. *Computers & Graphics* 44, 1 (2014), 1–10. https://doi.org/10.1016/j.cag.2014.07.004

Jan Bender, Dan Koschier, Tassilo Kugelstadt, and Marcel Weiler. 2017. A Micropolar Material Model for Turbulent SPH Fluids. In *ACM SIGGRAPH/Eurographics Symposium on Computer Animation (SCA '17)*. 1–8. https://doi.org/10.1145/3099564.3099578

Miklos Bergou, Max Wardetzky, David Harmon, Denis Zorin, and Eitan Grinspun. 2006. A Quadratic Bending Model for Inextensible Surfaces. In *Proceedings of the Fourth Eurographics Symposium on Geometry Processing (SGP '06)*. Eurographics Association, 227–230. https://doi.org/10.5555/1281957.1281987

Sofien Bouaziz, Sebastian Martin, Tiantian Liu, Ladislav Kavan, and Mark Pauly. 2014. Projective Dynamics: Fusing Constraint Projections for Fast Simulation. *ACM Transactions on Graphics* 33, 4 (2014), 1–11. https://doi.org/10.1145/2601097.2601116

George E. Brown and Rahul Narain. 2021. WRAPD: Weighted Rotation-Aware ADMM for Parameterization and Deformation. *ACM Transactions on Graphics* 40, 4, Article 82 (jul 2021), 14 pages. https://doi.org/10.1145/3450626.3459942

George E. Brown, Matthew Overby, Zahra Forootaninia, and Rahul Narain. 2018. Accurate Dissipative Forces in Optimization Integrators. *ACM Transactions on Graphics* 37, 6, Article 282 (dec 2018), 14 pages. https://doi.org/10.1145/3272127.3275011

Samuel R. Buss and Jay P. Fillmore. 2001. Spherical averages and applications to spherical splines and interpolation. *ACM Transactions on Graphics* 20, 2 (apr 2001), 95–126. https://doi.org/10.1145/502122.502124

Christian G. Böhmer, Patrizio Neff, and Belgin Seymenoğlu. 2016. Soliton-like solutions based on geometrically nonlinear Cosserat micropolar elasticity. *Wave Motion* 60 (jan 2016), 158–165. https://doi.org/10.1016/j.wavemoti.2015.09.006

Yunuo Chen, Minchen Li, Lei Lan, Hao Su, Yin Yang, and Chenfanfu Jiang. 2022. A Unified Newton Barrier Method for Multibody Dynamics. *ACM Transactions on Graphics* 41, 4, Article 66 (jul 2022), 14 pages. https://doi.org/10.1145/3528223.3530076

David Clyde, Joseph Teran, and Rasmus Tamstorf. 2017. Modeling and Data-Driven Parameter Estimation for Woven Fabrics. In *ACM SIGGRAPH/Eurographics Symposium on Computer Animation (SCA '17)*. Association for Computing Machinery, Article 17, 11 pages. https://doi.org/10.1145/3099564.3099577

Eugène Cosserat and François Cosserat. 1909. *Théorie des corps déformables.* A. Hermann et fils. English translation "Theory of Deformable Bodies" available by David H. Delphenich.

Michael A. Crisfield and Gordan Jelenić. 1999. Objectivity of strain measures in the geometrically exact three-dimensional beam theory and its finite-element implementation. *Proceedings of the Royal Society of London. Series A: Mathematical, Physical and Engineering Sciences* 455, 1983 (mar 1999), 1125–1147. https://doi.org/10.1098/rspa.1999.0352

Farzam Dadgar-Rad and Mokarram Hossain. 2023. A micropolar shell model for hard-magnetic soft materials. *Internat. J. Numer. Methods Engrg.* 124, 8 (2023), 1798–1817. https://doi.org/10.1002/nme.7188 arXiv:https://onlinelibrary.wiley.com/doi/pdf/10.1002/nme.7188

Crispin Deul, Tassilo Kugelstadt, Marcel Weiler, and Jan Bender. 2018. Direct Position-Based Solver for Stiff Rods. In *Computer Graphics Forum*. Wiley Online Library. https://doi.org/10.1111/cgf.13326

S. Diebels. 1999. A Micropolar Theory of Porous Media: Constitutive Modelling. *Transport in Porous Media* 34, 1/3 (1999), 193–208. https://doi.org/10.1023/a:1006517625933

V.A. Eremeyev, L.P. Lebedev, and H. Altenbach. 2012. *Foundations of Micropolar Mechanics.* Springer Berlin Heidelberg.

Ahmed Cemal Eringen. 1999. *Microcontinuum field theories: I. Foundations and Solids.* Springer Science & Business Media.

Zachary Ferguson, Minchen Li, Teseo Schneider, Francisca Gil-Ureta, Timothy Langlois, Chenfanfu Jiang, Denis Zorin, Danny M. Kaufman, and Daniele Panozzo. 2021. Intersection-Free Rigid Body Dynamics. *ACM Transactions on Graphics* 40, 4, Article 183 (jul 2021), 16 pages. https://doi.org/10.1145/3450626.3459802

José Antonio Fernández-Fernández, Fabian Löschner, Lukas Westhofen, Andreas Longva, and Jan Bender. 2023. SymX: Energy-based Simulation from Symbolic Expressions. (Feb. 2023). https://doi.org/10.48550/ARXIV.2303.02156 arXiv:2303.02156 [cs.CE]

Andreas Fischle and Patrizio Neff. 2017a. The geometrically nonlinear Cosserat micropolar shear-stretch energy. Part I: A general parameter reduction formula and energy-minimizing microrotations in 2D. *ZAMM - Journal of Applied Mathematics and Mechanics / Zeitschrift für Angewandte Mathematik und Mechanik* 97, 7 (jan 2017), 828–842. https://doi.org/10.1002/zamm.201500194

Andreas Fischle and Patrizio Neff. 2017b. The geometrically nonlinear Cosserat micropolar shear-stretch energy. Part II: Non-classical energy-minimizing microrotations in 3D and their computational validation. *ZAMM - Journal of Applied Mathematics and Mechanics* (2017). https://doi.org/10.1002/zamm.201600030

Stefan Fröhlich and Mario Botsch. 2011. Example-Driven Deformations Based on Discrete Shells. *Computer Graphics Forum* 30, 8 (aug 2011), 2246–2257. https://doi.org/10.1111/j.1467-8659.2011.01974.x

Theodore F. Gast, Craig Schroeder, Alexey Stomakhin, Chenfanfu Jiang, and Joseph M. Teran. 2015. Optimization Integrator for Large Time Steps. *IEEE Transactions on Visualization and Computer Graphics* 21, 10 (oct 2015), 1103–1115. https://doi.org/10.1109/tvcg.2015.2459687

Ionel-Dumitrel Ghiba, Gianluca Rizzi, Angela Madeo, and Patrizio Neff. 2022. Cosserat micropolar elasticity: classical Eringen vs. dislocation form. https://doi.org/10.48550/ARXIV.2206.02473 (Preprint).

P. Grammenoudis and Ch. Tsakmakis. 2005. Finite element implementation of large deformation micropolar plasticity exhibiting isotropic and kinematic hardening effects. *Internat. J. Numer. Methods Engrg.* 62, 12 (2005), 1691–1720. https://doi.org/10.1002/nme.1243

F. Sebastin Grassia. 1998. Practical Parameterization of Rotations Using the Exponential Map. *Journal of Graphics Tools* 3, 3 (mar 1998), 29–48. https://doi.org/10.1080/10867651.1998.10487493

Sara Grbčić, Adnan Ibrahimbegović, and Gordan Jelenić. 2018. Variational formulation of micropolar elasticity using 3D hexahedral finite-element interpolation with incompatible modes. *Computers & Structures* 205 (aug 2018), 1–14. https://doi.org/10.1016/j.compstruc.2018.04.005

Eitan Grinspun, Anil N. Hirani, Mathieu Desbrun, and Peter Schröder. 2003. Discrete Shells. In *ACM SIGGRAPH/Eurographics Symposium on Computer Animation (SCA '03)*. The Eurographics Association. https://doi.org/10.2312/SCA03/062-067

Du Q. Huynh. 2009. Metrics for 3D Rotations: Comparison and Analysis. *Journal of Mathematical Imaging and Vision* 35, 2 (June 2009), 155–164. https://doi.org/10.1007/s10851-009-0161-2

C. Kane, J. E. Marsden, M. Ortiz, and M. West. 2000. Variational integrators and the Newmark algorithm for conservative and dissipative mechanical systems. *Internat. J. Numer. Methods Engrg.* 49, 10 (2000), 1295–1325. https://doi.org/10.1002/1097-0207(20001210)49:10<1295::AID-NME993>3.0.CO;2-W

Ladislav Kavan and Jiří Žára. 2005. Spherical Blend Skinning: A Real-Time Deformation of Articulated Models. In *Proceedings of the 2005 Symposium on Interactive 3D Graphics and Games (I3D '05)*. Association for Computing Machinery, 9–16. https://doi.org/10.1145/1053427.1053429

Liliya Kharevych, Weiwei Yang, Yiying Tong, Eva Kanso, Jerrold E. Marsden, Peter Schröder, and Matthieu Desbrun. 2006. Geometric, Variational Integrators for Computer Animation. In *ACM SIGGRAPH/Eurographics Symposium on Computer Animation (SCA '06)*. The Eurographics Association. https://doi.org/10.2312/SCA/SCA06/043-051

Theodore Kim. 2020. A Finite Element Formulation of Baraff-Witkin Cloth. In *ACM SIGGRAPH/Eurographics Symposium on Computer Animation (SCA '20)*. Eurographics Association, Article 16, 9 pages. https://doi.org/10.1111/cgf.14111

Theodore Kim, Fernando De Goes, and Hayley Iben. 2019. Anisotropic Elasticity for Inversion-Safety and Element Rehabilitation. *ACM Transactions on Graphics* 38, 4, Article 69 (jul 2019), 15 pages. https://doi.org/10.1145/3306346.3323014

Theodore Kim and David Eberle. 2022. Dynamic Deformables: Implementation and Production Practicalities (Now with Code!). In *ACM SIGGRAPH 2022 Courses (SIGGRAPH '22)*. ACM, Article 7, 259 pages. https://doi.org/10.1145/3532720.3535628

Dan Kosloff and Gerald A. Frazier. 1978. Treatment of hourglass patterns in low order finite element codes. *International Journal for Numerical and Analytical Methods in Geomechanics* 2, 1 (1978), 57–72. https://doi.org/10.1002/nag.1610020105

Tassilo Kugelstadt, Dan Koschier, and Jan Bender. 2018. Fast Corotated FEM using Operator Splitting. *Computer Graphics Forum* 37, 8 (2018).

Tassilo Kugelstadt and Elmar Schömer. 2016. Position and Orientation Based Cosserat Rods. In *ACM SIGGRAPH/Eurographics Symposium on Computer Animation (SCA '16)*. The Eurographics Association, 1–10. https://doi.org/10.2312/SCA.20161234

Minchen Li, Zachary Ferguson, Teseo Schneider, Timothy Langlois, Denis Zorin, Daniele Panozzo, Chenfanfu Jiang, and Danny M. Kaufman. 2020. Incremental Potential Contact: Intersection-and Inversion-Free, Large-Deformation Dynamics. *ACM Transactions on Graphics* 39, 4, Article 49 (aug 2020), 20 pages. https://doi.org/10.1145/3386569.3392425

Minchen Li, Danny M. Kaufman, and Chenfanfu Jiang. 2021. Codimensional Incremental Potential Contact. *ACM Transactions on Graphics* 40, 4, Article 170 (jul 2021), 24 pages. https://doi.org/10.1145/3450626.3459767

Yijing Li and Jernej Barbic. 2014. Stable Orthotropic Materials. In *ACM SIGGRAPH/Eurographics Symposium on Computer Animation (SCA '14)*. The Eurographics Association. https://doi.org/10.2312/sca.20141121

Fabian Löschner, Andreas Longva, Stefan Jeske, Tassilo Kugelstadt, and Jan Bender. 2020. Higher-Order Time Integration for Deformable Solids. In *ACM SIGGRAPH/Eurographics Symposium on Computer Animation (SCA '20)*. Article 15, 13 pages. https://doi.org/10.1111/cgf.14110

Miles Macklin and Matthias Müller. 2021. A Constraint-Based Formulation of Stable Neo-Hookean Materials. In *ACM Motion in Games (MIG '21)*. Association for Computing Machinery, Article 12, 7 pages. https://doi.org/10.1145/3487983.3488289

Miles Macklin, Matthias Müller, and Nuttapong Chentanez. 2016. XPBD: Position-based Simulation of Compliant Constrained Dynamics. In *ACM Motion in Games (MIG '16)*. ACM, 49–54. https://doi.org/10.1145/2994258.2994272

Majid T. Manzari. 2004. Application of micropolar plasticity to post failure analysis in geomechanics. *International Journal for Numerical and Analytical Methods in Geomechanics* 28, 10 (jul 2004), 1011–1032. https://doi.org/10.1002/nag.356

Sebastian Martin, Peter Kaufmann, Mario Botsch, Eitan Grinspun, and Markus Gross. 2010. Unified Simulation of Elastic Rods, Shells, and Solids. *ACM Transactions on Graphics* 29, 4, Article 39 (jul 2010), 10 pages. https://doi.org/10.1145/1778765.1778776

Aleka McAdams, Yongning Zhu, Andrew Selle, Mark Empey, Rasmus Tamstorf, Joseph Teran, and Eftychios Sifakis. 2011. Efficient Elasticity for Character Skinning with Contact and Collisions. *ACM Transactions on Graphics* 30, 4, Article 37 (jul 2011), 12 pages. https://doi.org/10.1145/2010324.1964932

Kh. S. Mekheimer and M. A. El Kot. 2008. The micropolar fluid model for blood flow through a tapered artery with a stenosis. *Acta Mechanica Sinica* 24, 6 (aug 2008), 637–644. https://doi.org/10.1007/s10409-008-0185-7

Maher Moakher. 2002. Means and Averaging in the Group of Rotations. *SIAM J. Matrix Anal. Appl.* 24, 1 (2002), 1–16. https://doi.org/10.1137/S0895479801383877

Matthias Müller and Nuttapong Chentanez. 2011. Solid Simulation with Oriented Particles. *ACM Transactions on Graphics* 30, 4 (2011), 92:1–92:10. https://doi.org/10.1145/2010324.1964987

Matthias Müller, Bruno Heidelberger, Marcus Hennix, and John Ratcliff. 2006. Position Based Dynamics. In *Virtual Reality Interactions and Physical Simulations (VRIPHYS '06)*. Eurographics Association, 71–80. https://doi.org/10.2312/PE/vriphys/vriphys06/071-080

Ingo Münch. 2007. *Ein geometrisch und materiell nichtlineares Cosserat-Modell - Theorie, Numerik und Anwendungsmöglichkeiten*. Ph. D. Dissertation. Universität Karlsruhe.

Ingo Münch, Patrizio Neff, and Werner Wagner. 2011. A micropolar continuum model for large deformation caused by magnetic or electric fields. In *SPIE Proceedings*. SPIE. https://doi.org/10.1117/12.880568

Rahul Narain, Matthew Overby, and George E. Brown. 2016. ADMM ⊇ Projective Dynamics: Fast Simulation of General Constitutive Models. In *ACM SIGGRAPH/Eurographics Symposium on Computer Animation*. 1–8. https://doi.org/10.5555/2982818.2982822

Patrizio Neff. 2006. A finite-strain elastic-plastic Cosserat theory for polycrystals with grain rotations. *International Journal of Engineering Science* 44, 8 (2006), 574–594. https://doi.org/10.1016/j.ijengsci.2006.04.002

Patrizio Neff, Mircea Bîrsan, and Frank Osterbrink. 2015. Existence Theorem for Geometrically Nonlinear Cosserat Micropolar Model Under Uniform Convexity Requirements. *Journal of Elasticity* 121, 1 (feb 2015), 119–141. https://doi.org/10.1007/s10659-015-9517-6

Patrizio Neff, Kwon-Il Hong, and Jena Jeong. 2010. The Reissner-Mindlin plate is the Γ-limit of Cosserat elasticity. *Mathematical Models and Methods in Applied Sciences* 20, 09 (2010), 1553–1590. https://doi.org/10.1002/pamm.200910243

Oliver M. O'Reilly. 2017. *Kirchhoff's Rod Theory.* Springer International Publishing, Cham, 187–268. https://doi.org/10.1007/978-3-319-50598-5_5

M. Overby, G. E. Brown, J. Li, and R. Narain. 2017. ADMM ⊇ Projective Dynamics: Fast Simulation of Hyperelastic Models with Dynamic Constraints. *IEEE Transactions on Visualization and Computer Graphics* 23, 10 (Oct. 2017), 2222–2234. https://doi.org/10.1109/TVCG.2017.2730875

Dinesh K Pai. 2002. Strands: Interactive simulation of thin solids using cosserat models. In *Computer Graphics Forum*, Vol. 21. Wiley Online Library, 347–352. https://doi.org/10.1111/1467-8659.00594

W. Pietraszkiewicz and V.A. Eremeyev. 2009. On natural strain measures of the non-linear micropolar continuum. *International Journal of Solids and Structures* 46, 3-4 (feb 2009), 774–787. https://doi.org/10.1016/j.ijsolstr.2008.09.027

Alessio Quaglino. 2012. *Membrane locking in discrete shell theories.* Ph. D. Dissertation. Universität Göttingen. https://doi.org/10.53846/goediss-2533

S. Ramezani, R. Naghdabadi, and S. Sohrabpour. 2009. Constitutive equations for micropolar hyper-elastic materials. *International Journal of Solids and Structures* 46, 14 (2009), 2765–2773. https://doi.org/10.1016/j.ijsolstr.2008.10.009

Oliver Sander. 2012. Geodesic finite elements on simplicial grids. *Internat. J. Numer. Methods Engrg.* 92, 12 (jun 2012), 999–1025. https://doi.org/10.1002/nme.4366

Oliver Sander. 2015. Geodesic finite elements of higher order. *IMA J. Numer. Anal.* 36, 1 (05 2015), 238–266. https://doi.org/10.1093/imanum/drv016

Oliver Sander, Patrizio Neff, and Mircea Birsan. 2016. Numerical treatment of a geometrically nonlinear planar Cosserat shell model. *Computational Mechanics* 57, 5 (feb 2016), 817–841. https://doi.org/10.1007/s00466-016-1263-5

Carlo Sansour and Werner Wagner. 2003. Multiplicative updating of the rotation tensor in the finite element analysis of rods and shells - a path independent approach. *Computational Mechanics* 31, 1-2 (may 2003), 153–162. https://doi.org/10.1007/s00466-002-0401-4

P. Schmidt, J. Born, D. Bommes, M. Campen, and L. Kobbelt. 2022. TinyAD: Automatic Differentiation in Geometry Processing Made Simple. *Computer Graphics Forum* 41, 5 (2022), 113–124. https://doi.org/10.1111/cgf.14607

Christian Schumacher, Bernhard Thomaszewski, Stelian Coros, Sebastian Martin, Robert Sumner, and Markus Gross. 2012. Efficient Simulation of Example-Based Materials. In *ACM SIGGRAPH/Eurographics Symposium on Computer Animation (SCA '12)*. The Eurographics Association. https://doi.org/10.2312/SCA/SCA12/001-008

Lee Shunn and Frank Ham. 2012. Symmetric quadrature rules for tetrahedra based on a cubic close-packed lattice arrangement. *J. Comput. Appl. Math.* 236, 17 (2012), 4348–4364. https://doi.org/10.1016/j.cam.2012.03.032

Eftychios Sifakis and Jernej Barbic. 2012. FEM Simulation of 3D Deformable Solids. In *ACM SIGGRAPH 2012 Courses*. ACM, 1–50. https://doi.org/10.1145/2343483.2343501

Breannan Smith, Fernando De Goes, and Theodore Kim. 2018. Stable Neo-Hookean Flesh Simulation. *ACM Transactions on Graphics* 37, 2 (mar 2018), 1–15. https://doi.org/10.1145/3180491

Joan Solà. 2017. Quaternion kinematics for the error-state Kalman filter. https://doi.org/10.48550/ARXIV.1711.02508

Jonas Spillmann and Matthias Teschner. 2007. CORDE: Cosserat Rod Elements for the Dynamic Simulation of One-Dimensional Elastic Objects. In *ACM SIGGRAPH/Eurographics Symposium on Computer Animation (SCA '07)*. Eurographics Association, 63–72. https://doi.org/10.2312/SCA/SCA07/063-072

Jonas Spillmann and Matthias Teschner. 2009. Cosserat Nets. *IEEE Transactions on Visualization and Computer Graphics* 15, 2 (mar 2009), 325–338. https://doi.org/10.1109/tvcg.2008.102

P. Steinmann and E. Stein. 1997. A unifying treatise of variational principles for two types of micropolar continua. *Acta Mechanica* 121, 1-4 (mar 1997), 215–232. https://doi.org/10.1007/bf01262533

Alexey Stomakhin, Russell Howes, Craig Schroeder, and Joseph M. Teran. 2012. Energetically Consistent Invertible Elasticity. In *ACM SIGGRAPH/Eurographics Symposium on Computer Animation (SCA '12)*. Eurographics Association, 25–32.

Josip Tambača and Igor Velčić. 2010. Existence theorem for nonlinear micropolar elasticity. *ESAIM: Control, Optimisation and Calculus of Variations* 16, 1 (1 2010), 92–110. https://doi.org/10.1051/cocv:2008065

Ty Trusty, Danny Kaufman, and David I.W. Levin. 2022. Mixed Variational Finite Elements for Implicit Simulation of Deformables. In *SIGGRAPH Asia 2022 Conference Papers*. ACM. https://doi.org/10.1145/3550469.3555418

Nobuyuki Umetani, Ryan Schmidt, and Jos Stam. 2014. Position-based Elastic Rods. In *ACM SIGGRAPH/Eurographics Symposium on Computer Animation (SCA '14)*. ACM, 21–30. https://doi.org/10.1145/2614106.2614158

Stuart Walsh and Antoinette Tordesillas. 2006. Finite element methods for micropolar models of granular materials. *Applied Mathematical Modelling* 30 (10 2006), 1043–1055. https://doi.org/10.1016/j.apm.2005.05.016

Hongyi Xu and Jernej Barbič. 2017. Example-Based Damping Design. *ACM Transactions on Graphics* 36, 4, Article 53 (jul 2017), 14 pages. https://doi.org/10.1145/3072959.3073631

Hongyi Xu, Funshing Sin, Yufeng Zhu, and Jernej Barbič. 2015. Nonlinear Material Design Using Principal Stretches. *ACM Transactions on Graphics* 34, 4, Article 75 (July 2015), 11 pages. https://doi.org/10.1145/2766917